



JIM HUNTER

<https://turystyka.wp.pl>

*Co wiemy o implantacji ciężkich jonów?  
Czy występuje „efekt dalekiego zasięgu”?*

# What do we know about heavy ion implantation? Is there a „long-range effect?”

*Co wiemy o implantacji ciężkich jonów?  
Czy występuje „efekt dalekiego zasięgu”?*



J.Dryzek, P. Horodek

Institute of Nuclear Physics Polish Academy of Sciences, PL-31342 Krakow, Poland  
Joint Institute for Nuclear Research, Joliot-Curie 6, 141980 Dubna, Russia



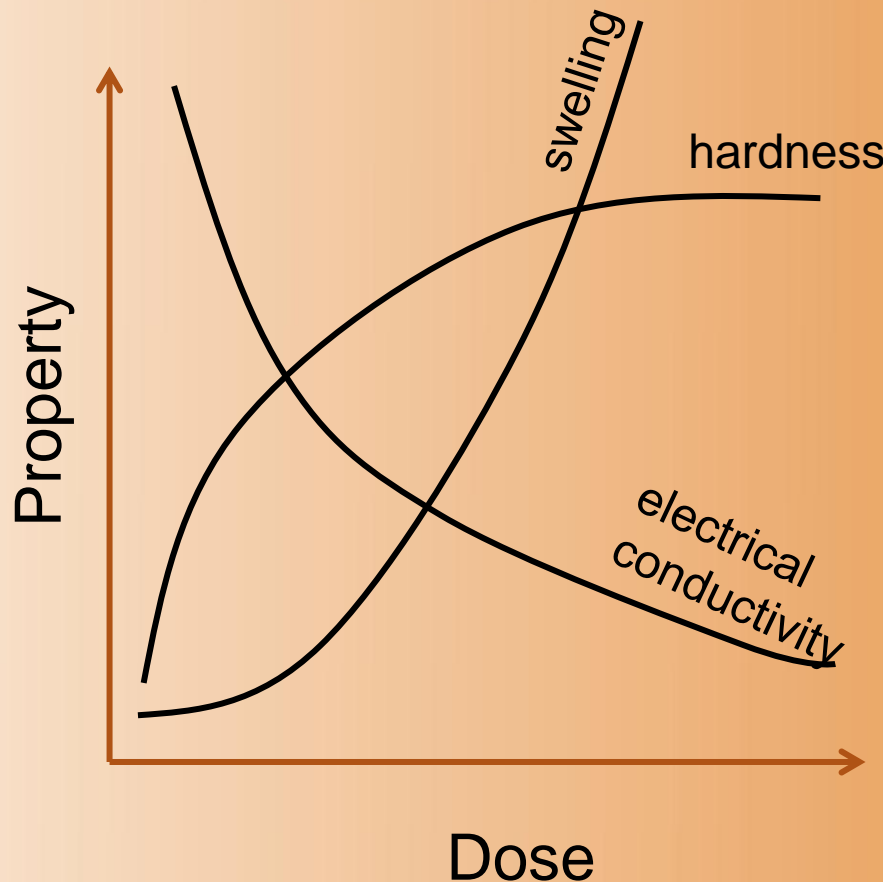
# Outline

- **Ion implantation process**
  - Stopping power
  - Damage and defects
- **What is a long-range effect (LRE)**
  - Experimental observation
  - Positron results for LRE
- **Positron experiments for searching of LRE**
  - VEP results
  - Etching technique
- **Conclusions**

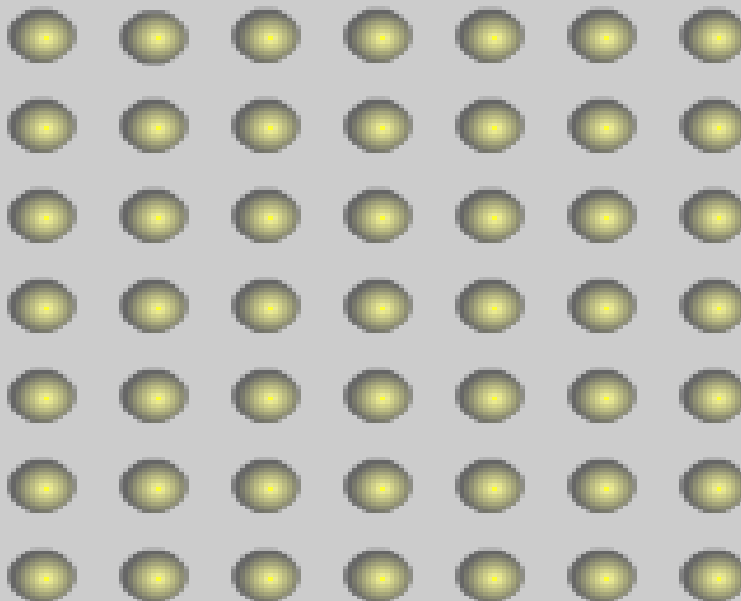
# Ion implantation process

**During implantation** the transfer of energy from an incident projectile to the solid takes place. It results in distribution of displacement of host atoms and/or generation of other defects.

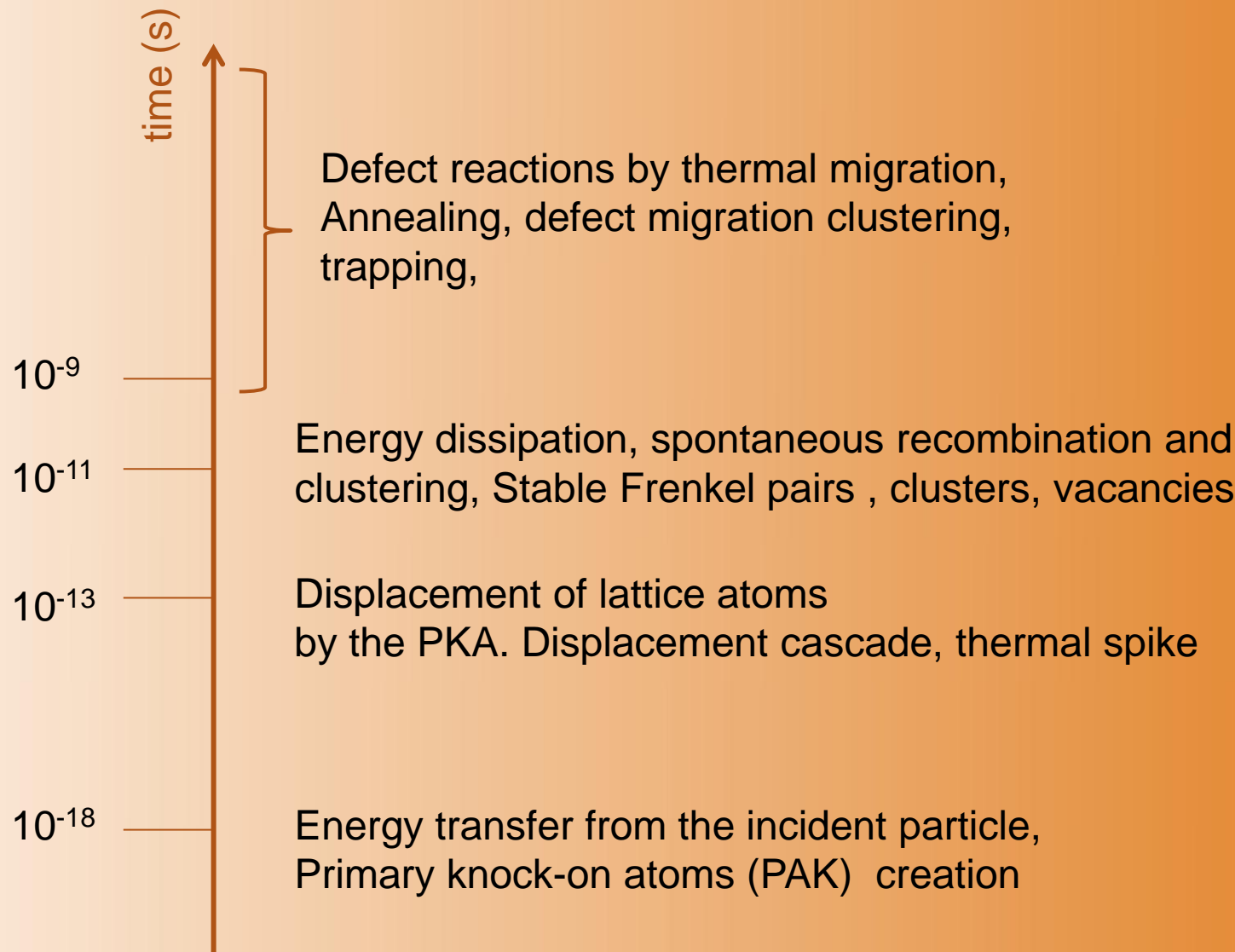
## Dose dependence of different properties



## Ion implantation: Frenkel pair



## Approximate time-scale for the production of defects in irradiated metals



## Stopping power describes the loss of projectile kinetic energy

The radiation damage event is defined as the transfer of energy from an incident projectile to the solid and the resulting distribution of target atoms after completion of the event.

Energy loss per unit length  $-dE/dx$ , or divided the atom number density it is the stopping power:

$$\left( -\frac{dE}{dx} \right)_{total} = \left( -\frac{dE}{dx} \right)_{elastic(nuclear)} + \left( -\frac{dE}{dx} \right)_{electronic(ionization)} + \left( -\frac{dE}{dx} \right)_{radiation}$$

Subsequent events involving the migration of the point defects and defect clusters and additional clustering or dissolution of the clusters are classified as **radiation damage effects**.

## Electronic stopping power of several ions in Si

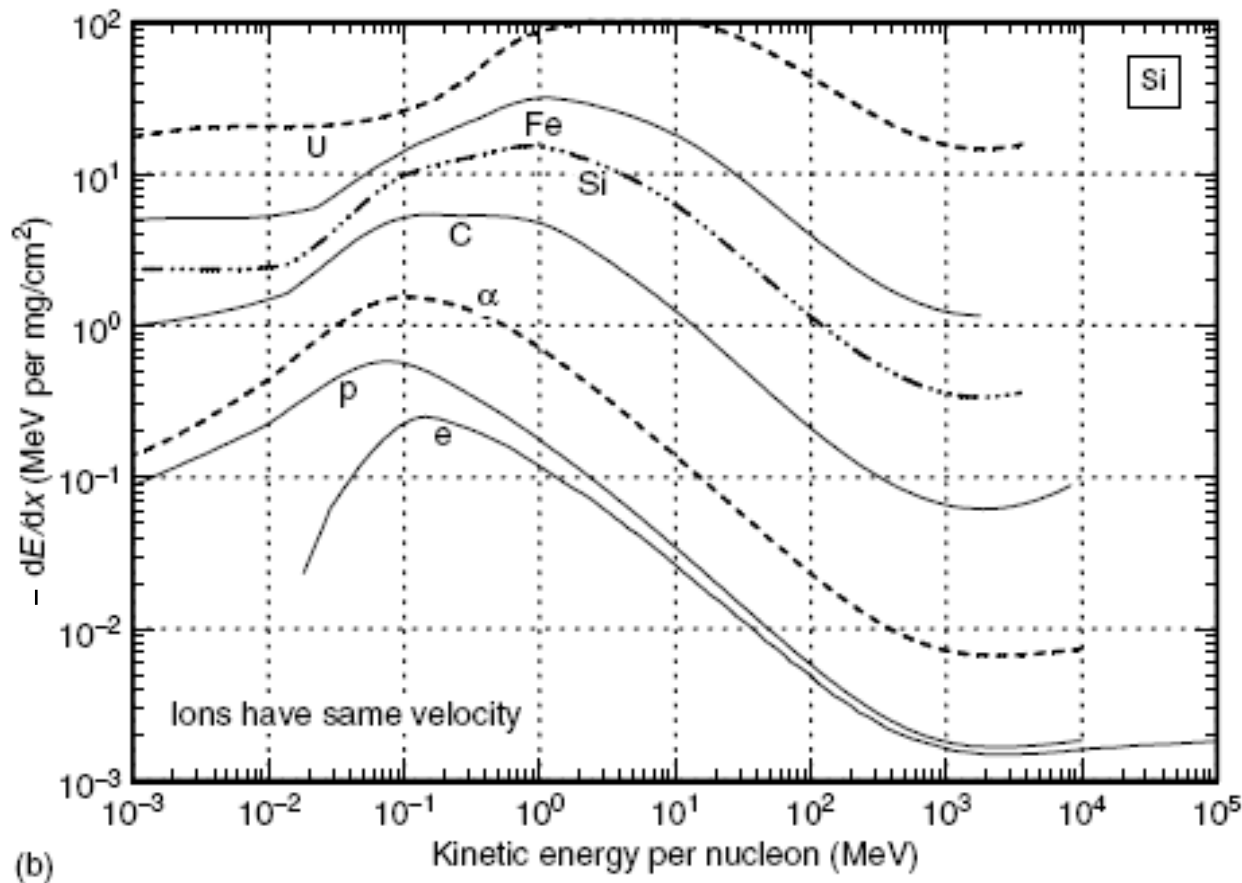
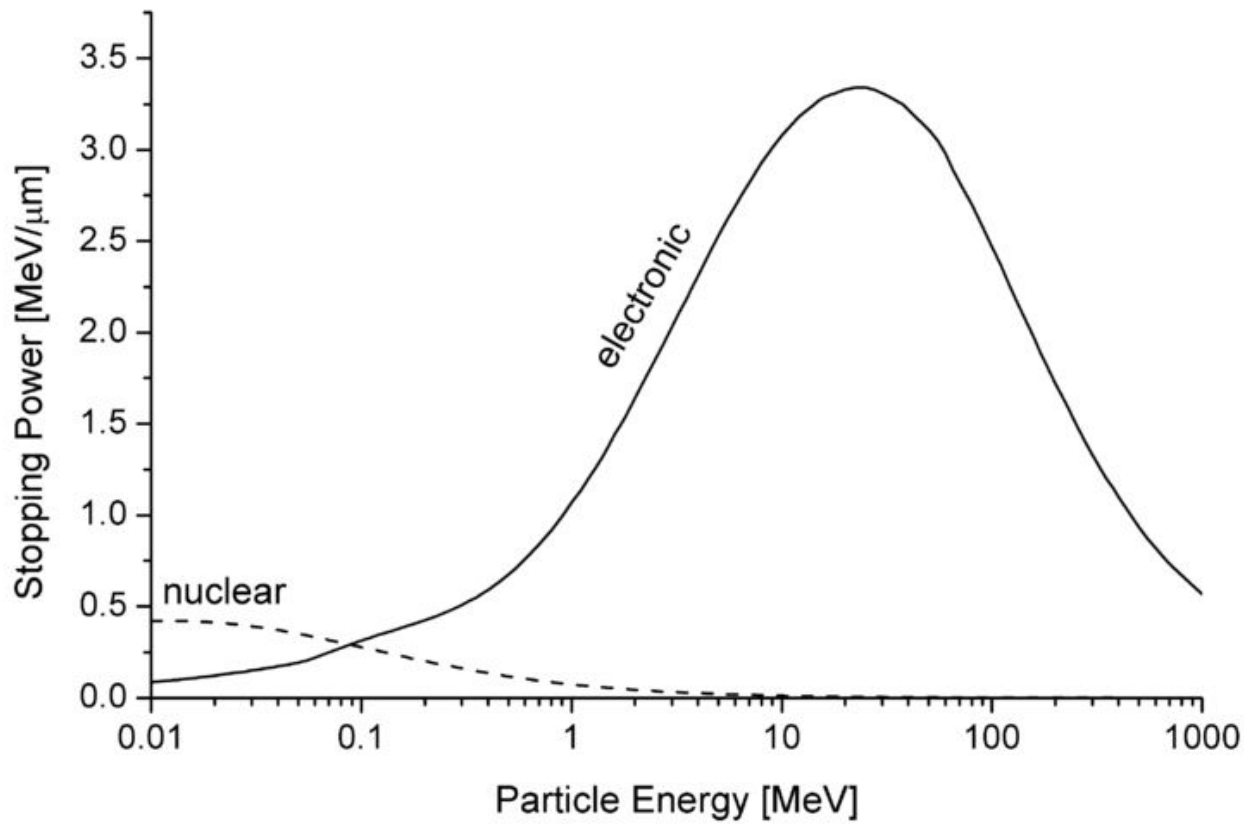
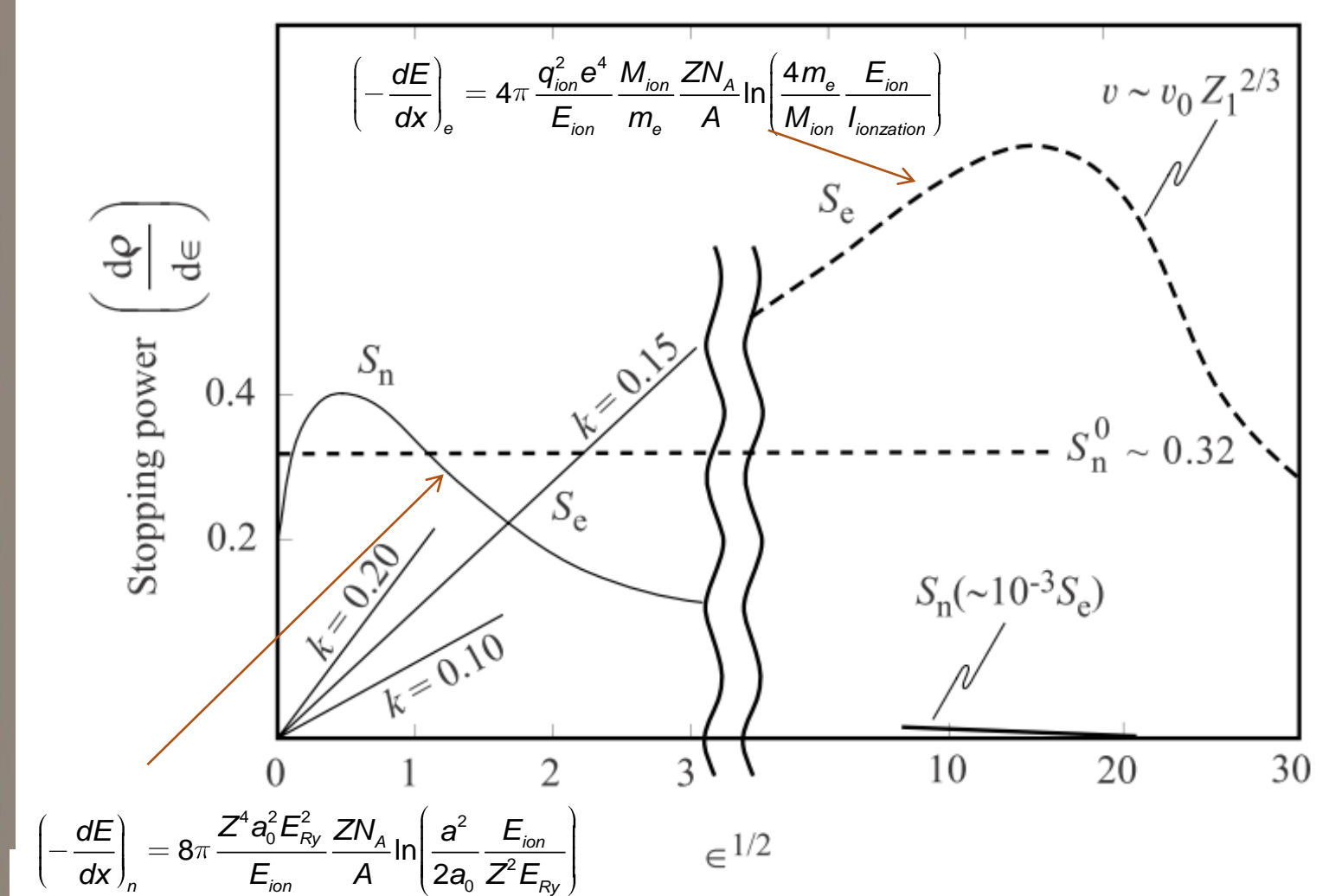


**FIGURE 4.2** (a) Stopping powers of an electron, proton, alpha particle, and carbon, silicon, iron, and uranium ions in silicon, as a function of their kinetic energies. (b) As a function of their velocities. ( $e$  data from NIST. Ion data from SRIM.)

## Electronic and nuclear stopping power



## Electronic and nuclear stopping power as a function of ion energy



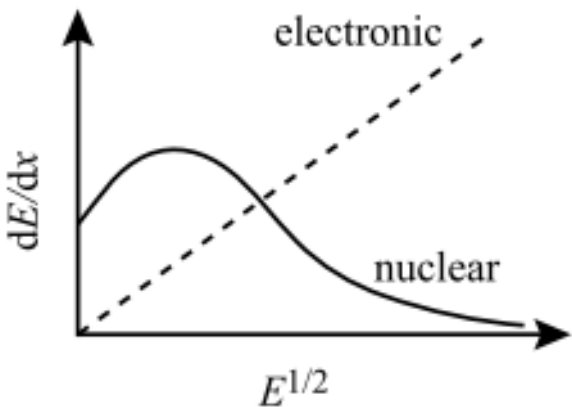


**Fig. 2.23.** Variation in nuclear and electronic stopping powers over the energy range of relevance to ion–solid interactions

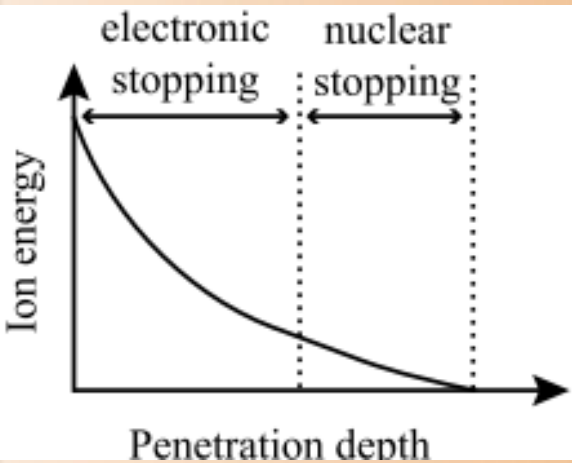
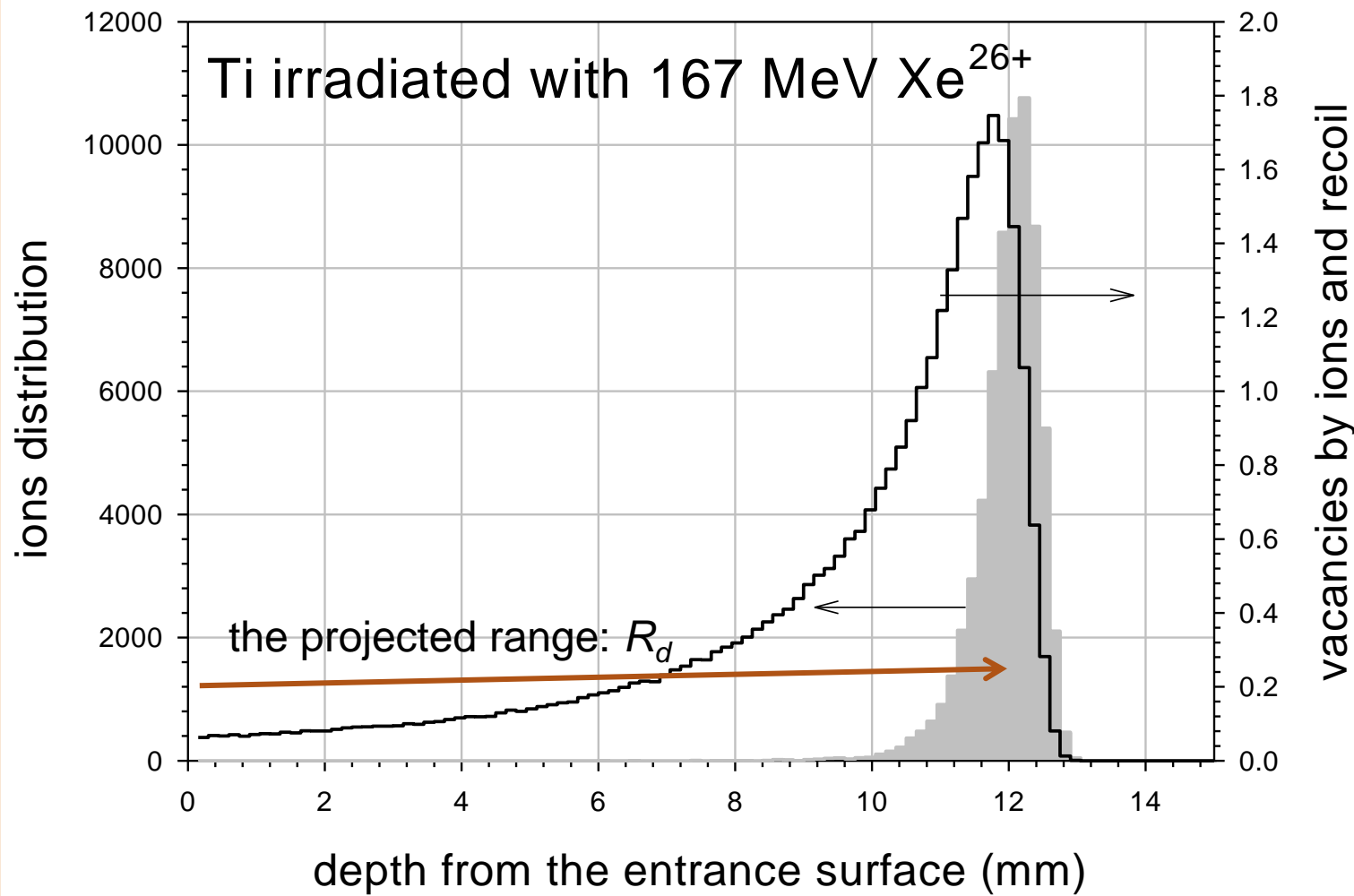


**Fig. 2.24.** Residual range of an ion incident on a target and the regimes of electronic and nuclear stopping dominance

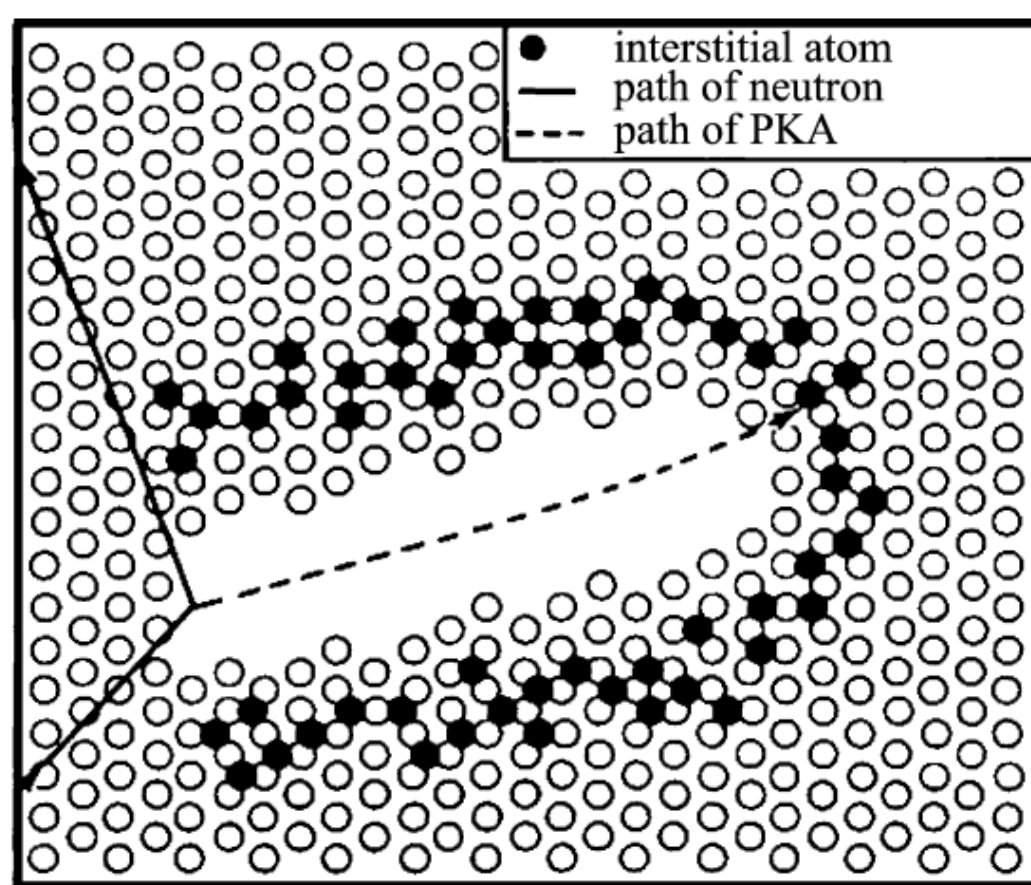
## Damage morphology, displacement efficiency and average recoil energy for 1MeV particles of different type incident on nickel

projectiles	trajectory, defects	defect production efficiency	average recoil energy
1MeV electrons	Frenkel pair	50-100%	60 eV
1MeV protons	small clusters	25 %	200 eV
1 MeV heavy ions	cluster	4 %	5 keV
1 MeV neutrons	cluster	2 %	35 keV

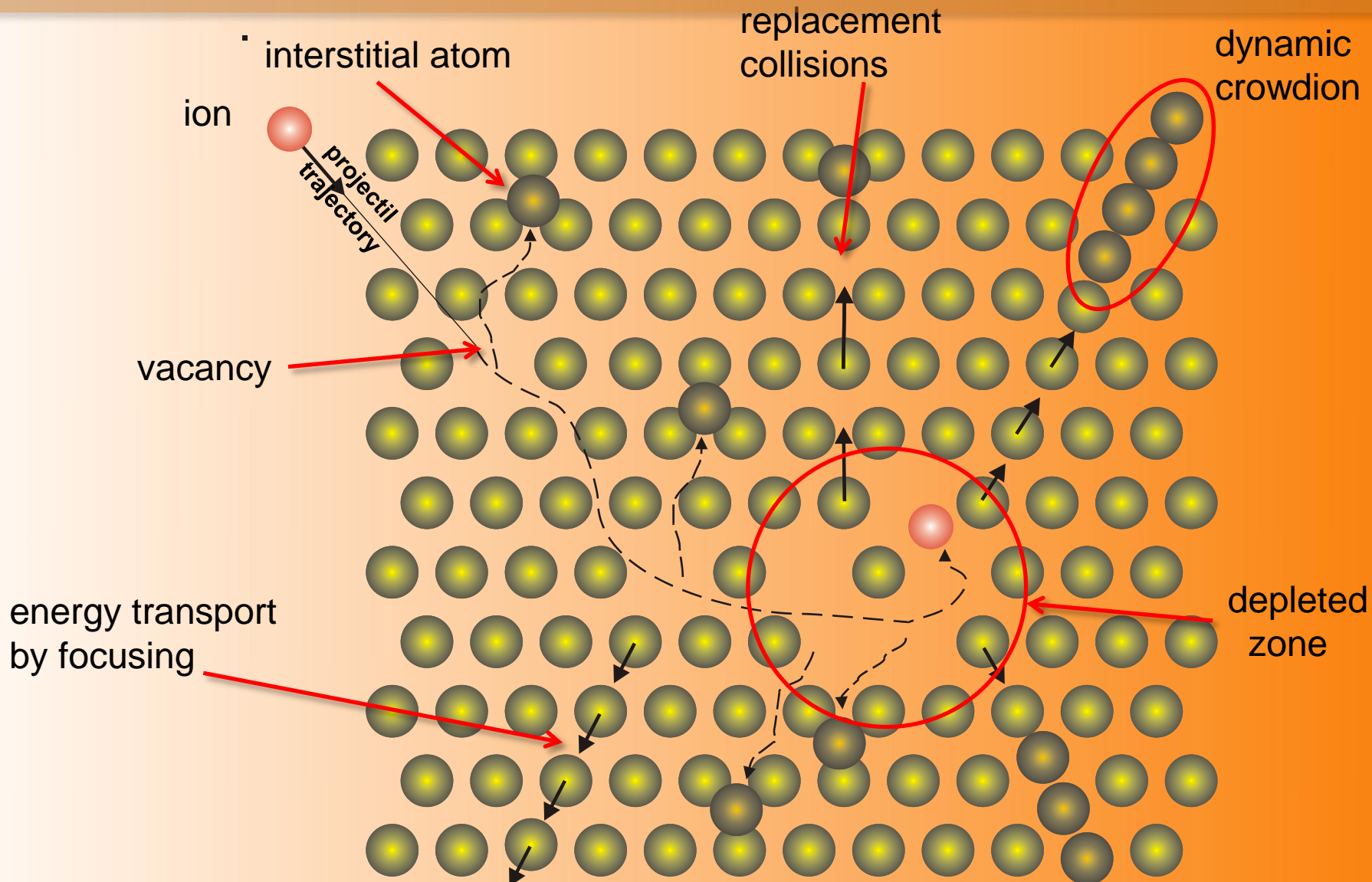
## SRIM, trajectory simulations of Xe ions in Ti



## Original version of the displacement spike as drawn by Brinkman



# Displacement spike as drawn accounting for crystallinity in the damage cascade



## Dislocation loops, vacancy clusters

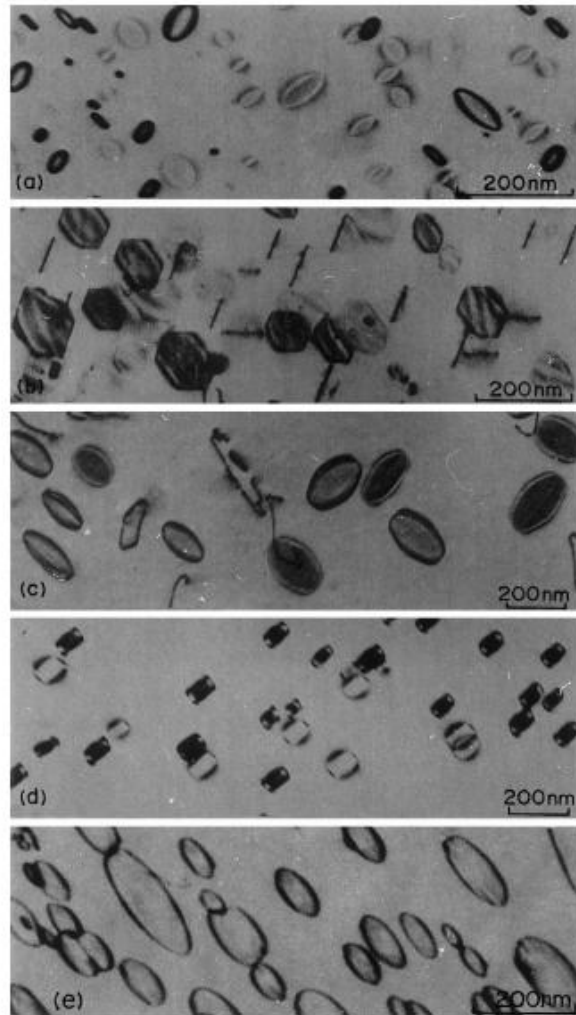


Fig. 3. Interstitial type dislocation loops produced in various metals by electron irradiation at temperatures above the recovery stage III [15]. Faulted loops on  $\{111\}$  planes in (a) Aluminum, (b) copper, and (c) nickel. Perfect loops on  $\{100\}$  planes in (d) iron, and loops on basal plane in (e) zinc.

Al.

Cu

Ni

Fe

Zn

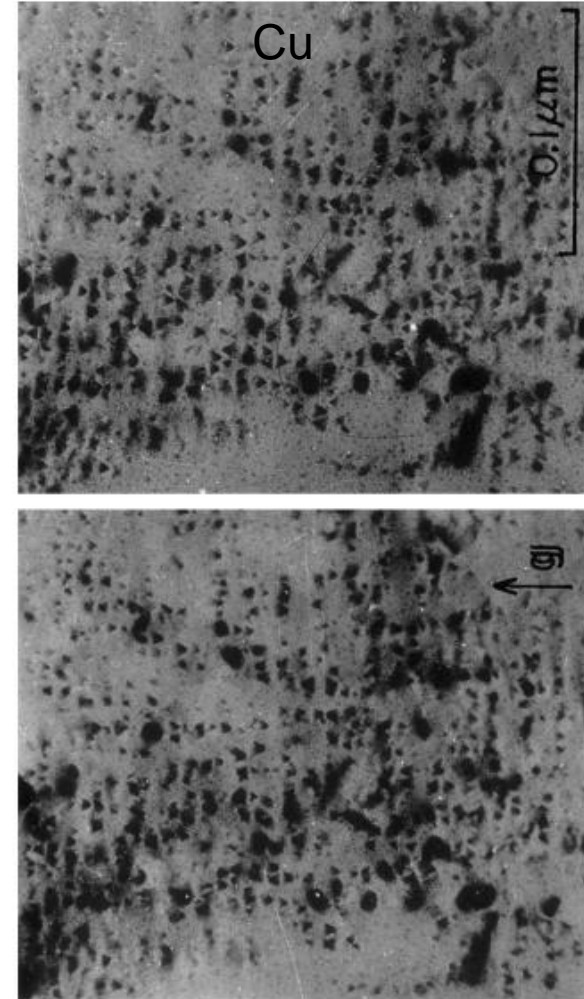


Fig. 4. Stereoscopic pair micrographs of vacancy clusters in the shape of stacking fault tetrahedra in copper electron irradiated at 310 K [26]. All SFT are located within a thin layer beneath the electron incident surface. This is considered to be due to the enrichment of vacancies along the surface caused by the transport of interstitials into the deeper position from the surface.

## Dislocation loops, vacancy clusters in Fe after neutron irradiation

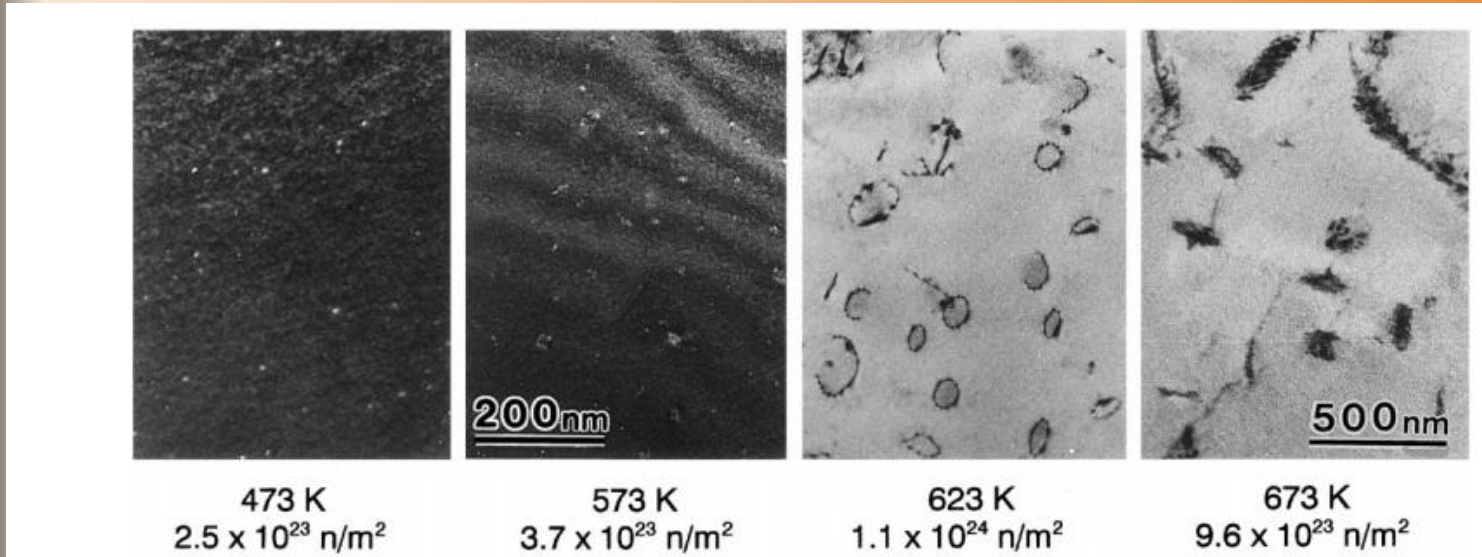
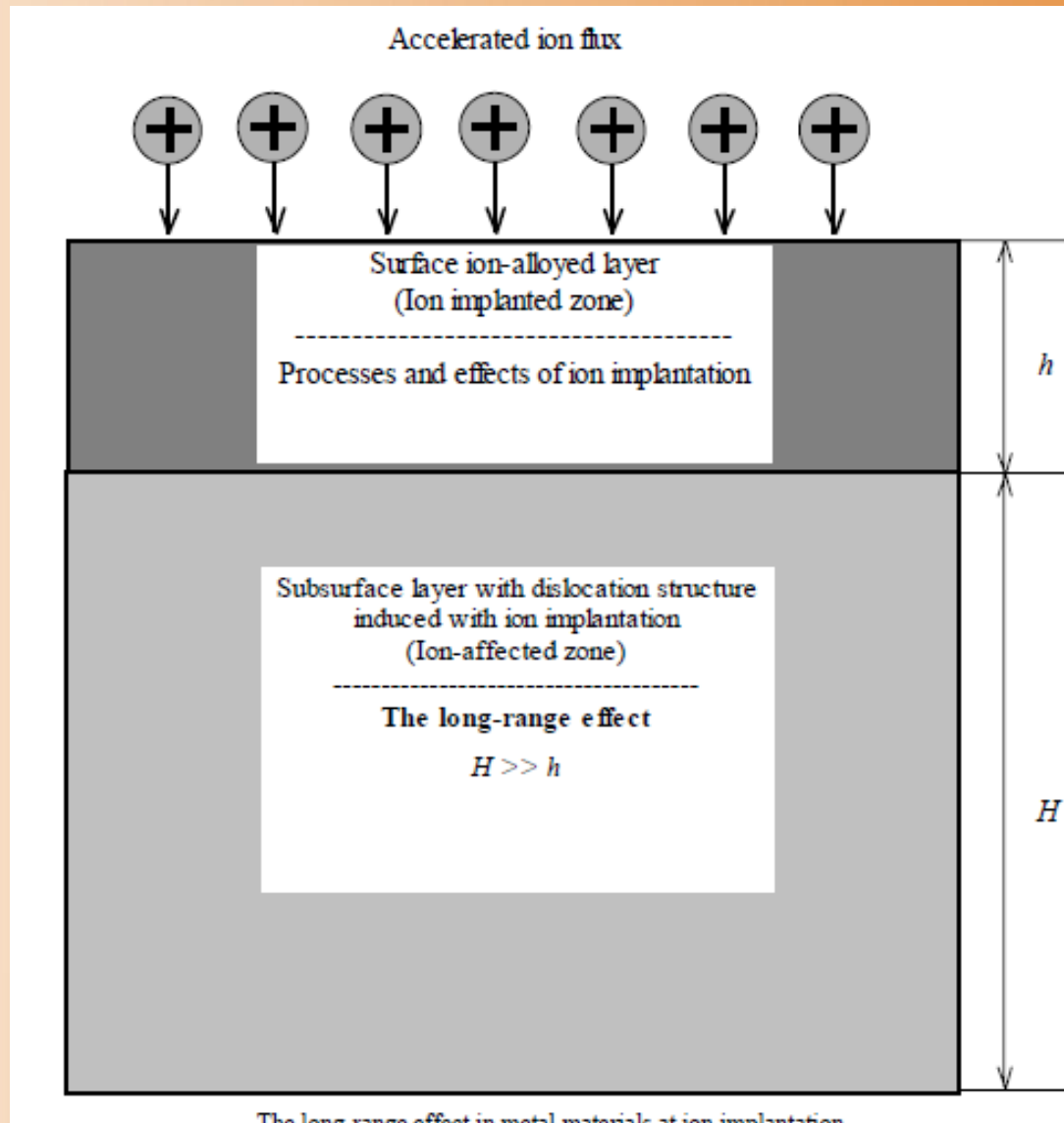


Fig. 1. Defect structures of iron neutron-irradiated at four temperatures. Images of specimens irradiated at 473 and 573 K have the same magnification and images of specimens irradiated at 623 and 673 K have the same magnification.

# A long-range effect (LRE)

Authors reported another effect accompanying implantation, i.e., a damage region is extended much deeper into material than the range of implanted ions.

## What is a long-range effect (LRE) ?



Cu

## LRE in Cu

$R_p < 0.04 \mu\text{m}$

Cu implanted with  
72-130 keV  
Ni ions

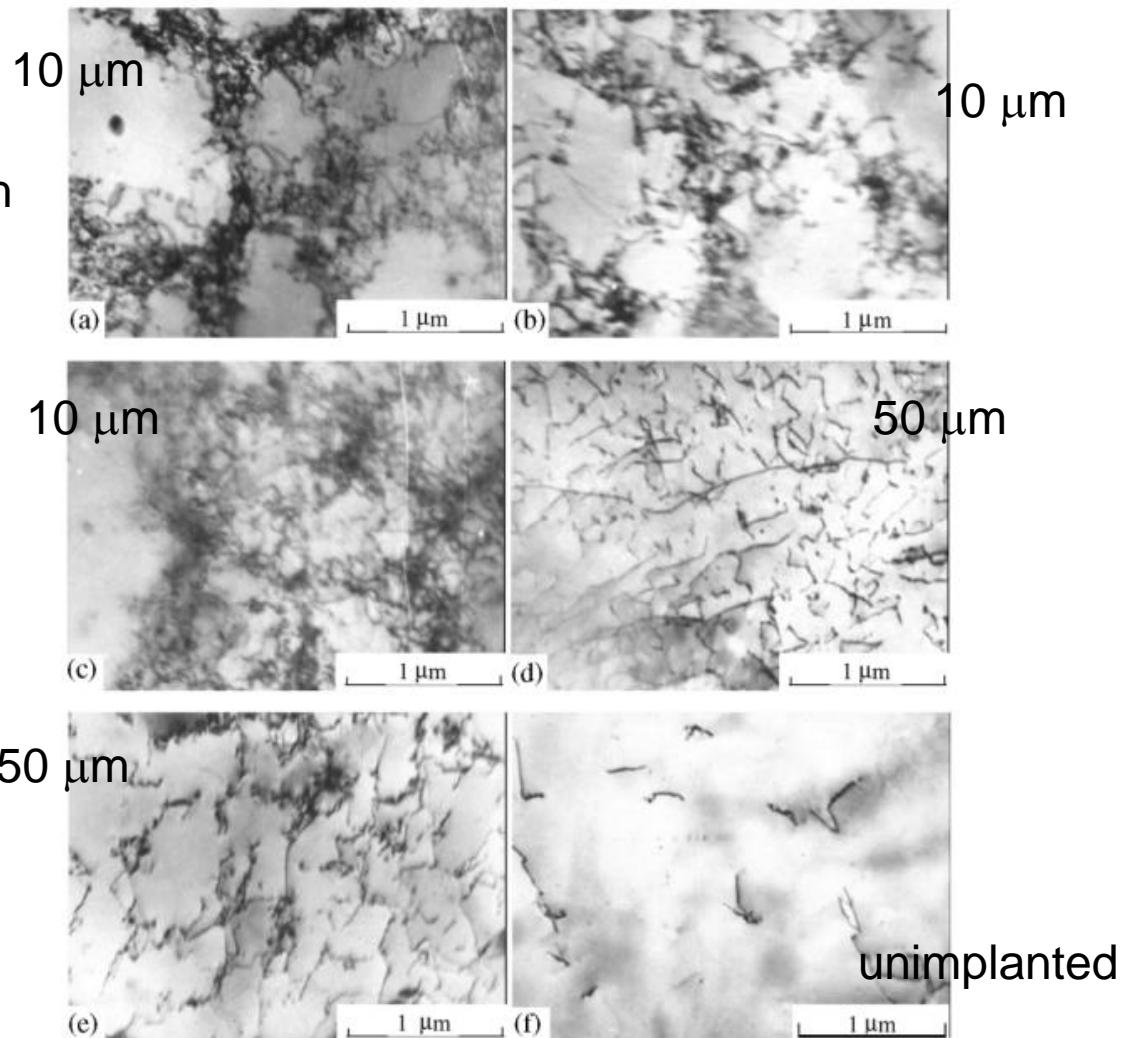


Fig. 3. Dislocation structures formed in Cu implanted with the Ni ions (a-e); the ion implanted dose is ( $\text{ion}\cdot\text{cm}^{-2}$ ): (a-d)  $2 \times 10^{17}$ , (f)  $4.6 \times 10^{17}$ ; the distance to the irradiated surface is ( $\mu\text{m}$ ): (a-c) 10; (d-e) 50; the target temperature (K) is: (a) 343; (b) 523; (c-e) 423; and (f) dislocation structure in unimplanted Cu.

## LRE in Cu

Cu

Ti and Zr ions were implanted into Cu. The ion energy was about 100 keV and the applied (incident) dose was  $10^{17}$  ions/cm<sup>2</sup>.

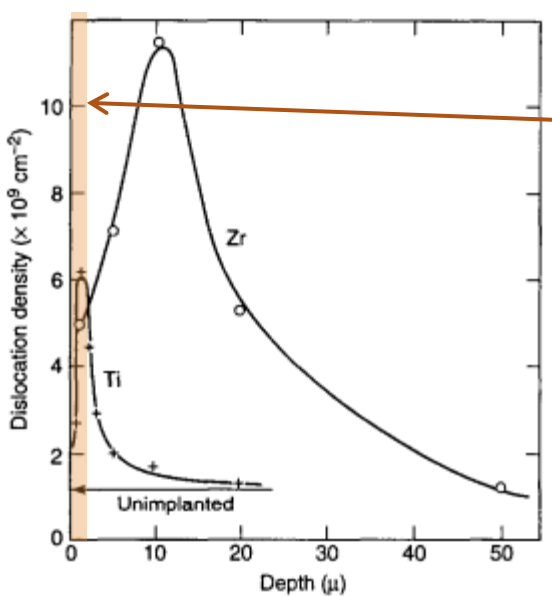


Fig. 5. Dependence of scalar dislocation density on distance below the surface of Zr implanted Cu and Ti implanted Cu. The dislocation density of unimplanted Cu (i.e., the initial state) is indicated.

Ion projected range:

$$R_p = 0.037 \text{ } \mu\text{m for Ti ions}$$
$$0.025 \text{ } \mu\text{m for Zr ions}$$

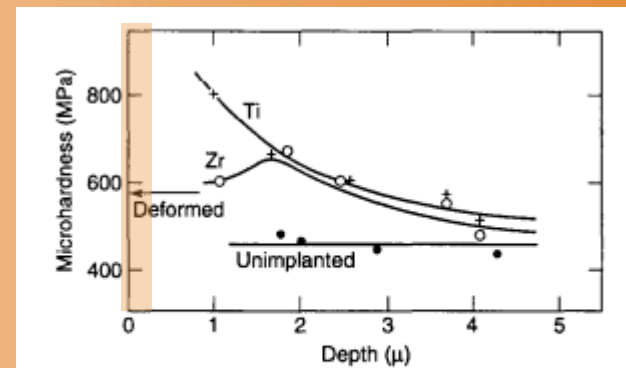


Fig. 6. Dependence of microhardness on the depth of indentation for unimplanted Cu, Zr implanted Cu, and Ti implanted Cu. The microhardness of Cu deformed by a single-axis compression of 6% is indicated (580 MPa).

*Ti and Zr ion implantations produce a developed dislocation structure in the Cu subsurface layers the thickness of which is 2 to 3 order of magnitude greater than the thickness of the implanted layer.*

## LRE explanation

*Static and dynamic stresses generated in a target at ion implantation play the determining role in an accumulation of dislocations in the ion-affected zone and in the long-range effect manifestation.*

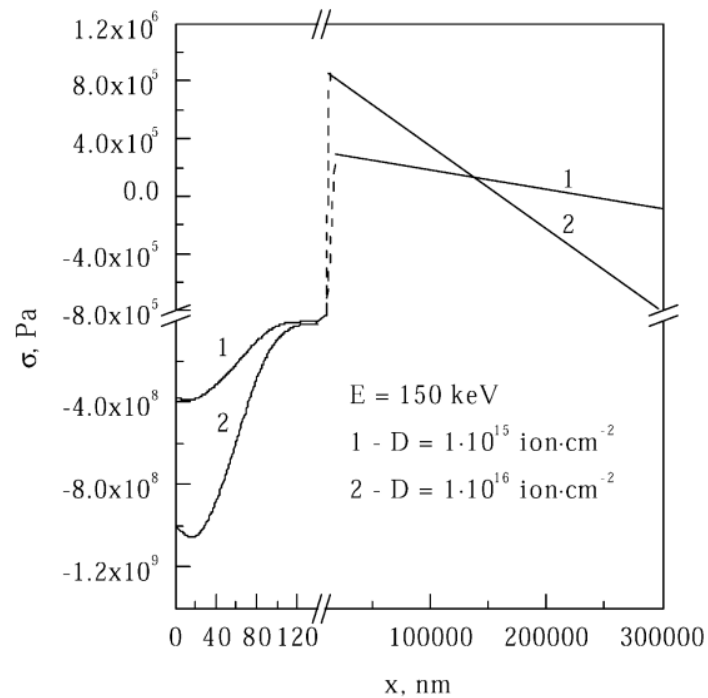
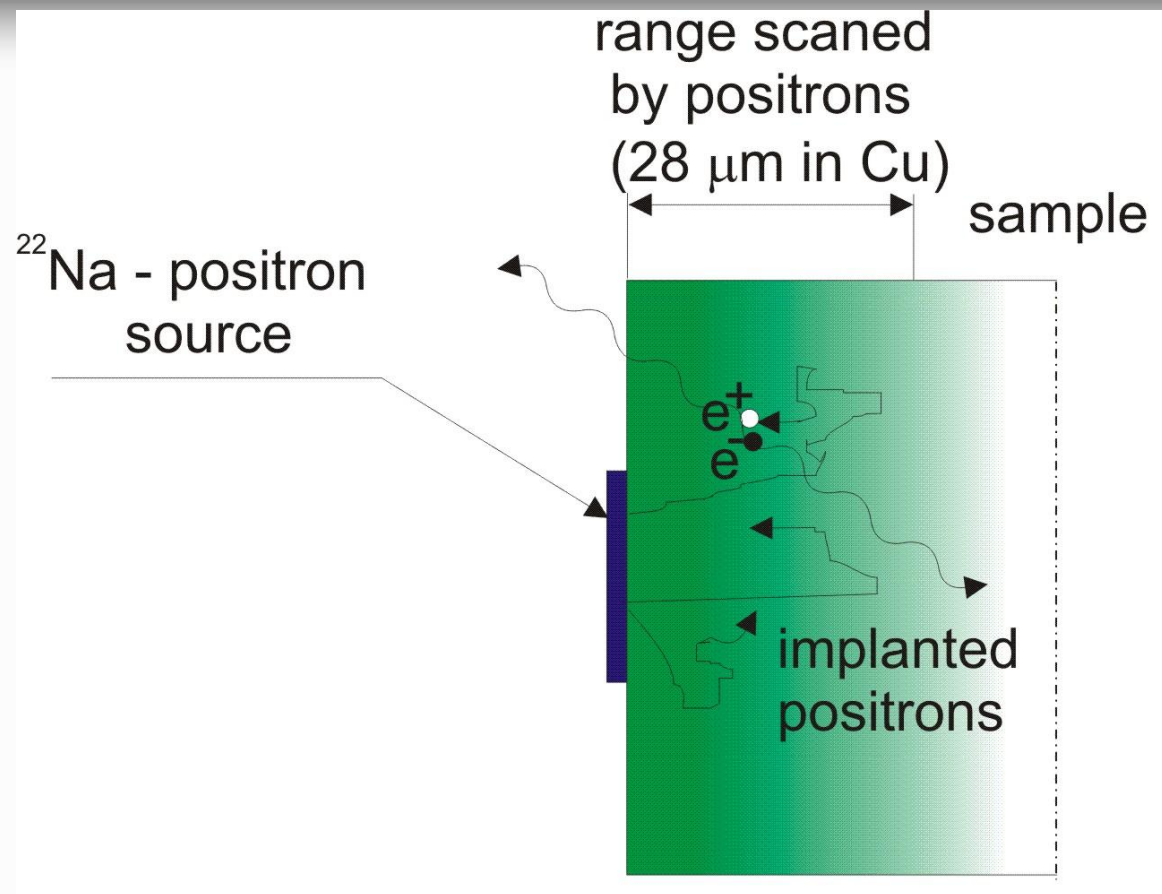
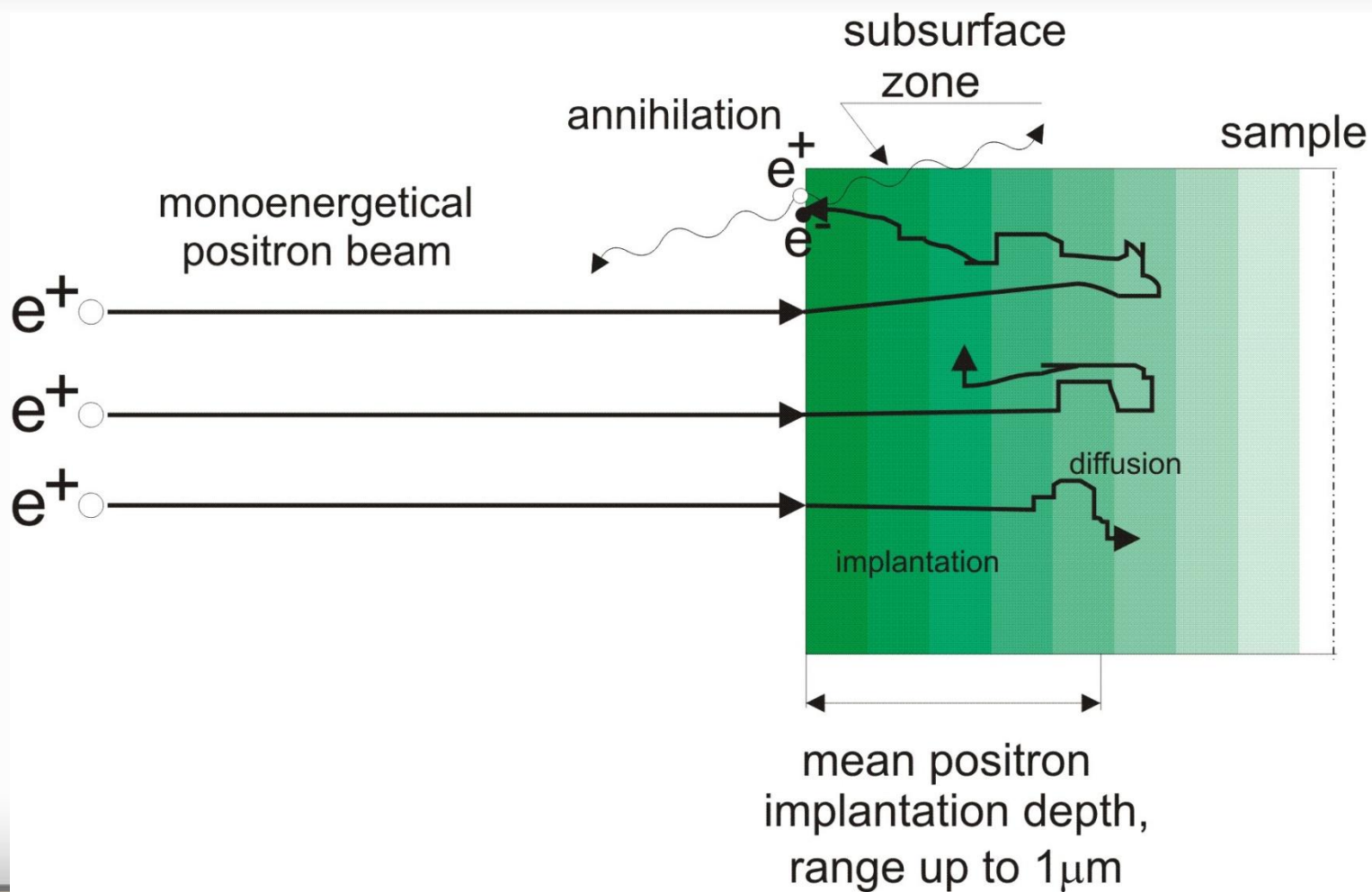


Fig. 9. The dependence of the mechanical stresses generated in the implanted zone and the ion-affected zone of  $\alpha$ -Fe by implantation of the Ar ions on the distance from the irradiated surface.

## Conventional experiments with $^{22}\text{Na}$ positrons



## Variable energy positron beam (VEP) measurement



## LRE is not always observed.

Si

L. Liszkay et.al., Appl. Surf. Scien. **194**, 136 (2002)

VEP and XTEM experiment, Si (100) irradiated with 18 keV He,  
dose  $2\text{-}3 \times 10^{16}$  ions/cm<sup>2</sup>

$R_p=190$  nm, and depth of observed by XTEM voids 180-240  
nm.

*Good agreement with the depth range of positron traps.*

## LRE in positron experiments

Fe

SiC

A.Kinomura, R. Suzuki, T. Ohdaira, N. Oshima, K. Ito, Y. Kobayashi, T. Iwai, *J. Phys.: Conf. Series*, **262**, 012029 (2011).

VEP experiment; Fe irradiated with 150 keV Ar<sup>+</sup>.

*The difference between the measured and simulated profiles was observed even in the case of the Fe sample irradiated at 100 K where vacancies are immobile. The origin of such differences cannot be explained by vacancy diffusion, errors of positron implantation depths and recoils from the surface impurities.*

W. Anwand, G. Brauer, W. Skorupa, *Appl. Surf. Scien.* **194**, 131 (2002).

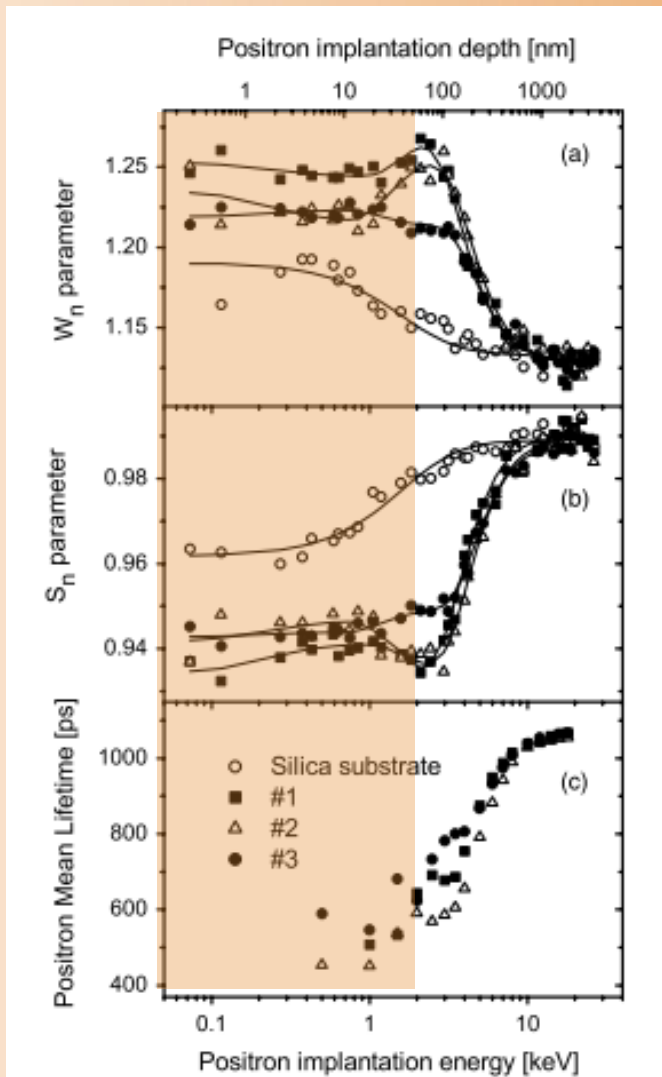
VEP experimental; 6H-SiC, implanted with 65 keV Al<sup>+</sup> and 120 keV N<sup>+</sup>.

*Vacancy-type defects reach much deeper into the material than the range of implanted ions as estimated from TRIM calculations.*

VEP -variable energy positron beam

## VEP results which inticates LRE

Silica  
glass



Silica glass plates were implanted at room temperature with  $\text{Ar}^+$  ions at 30 keV with a dose of  $1 \times 10^{17}$  ions/cm<sup>2</sup>, 50 keV with a dose of  $1 \times 10^{17}$  and  $1.5 \times 10^{17}$  ions/cm<sup>2</sup> and

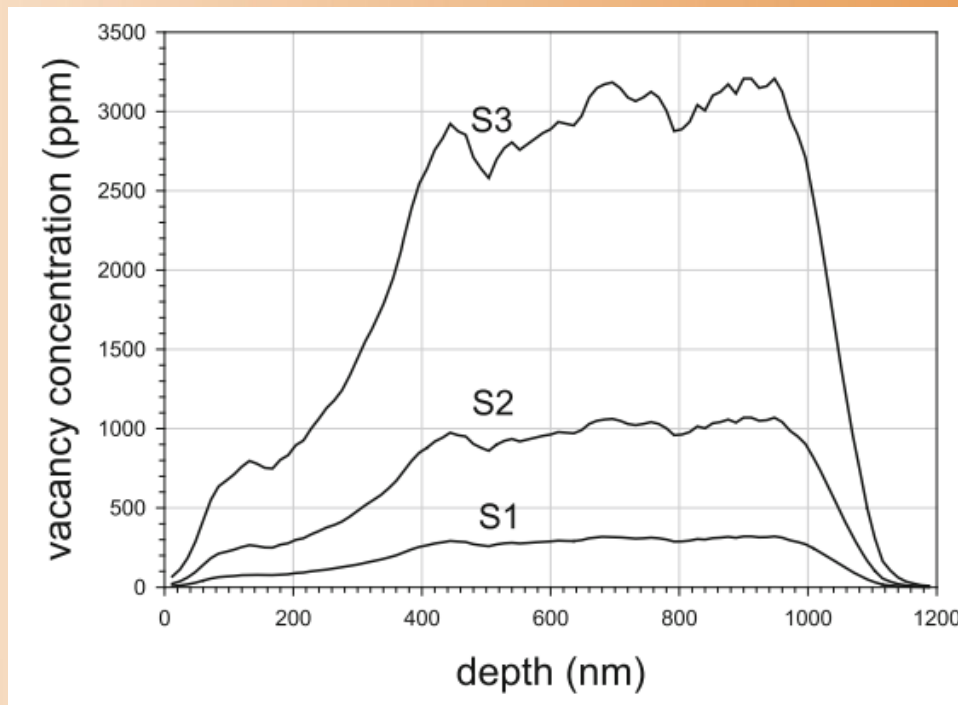
Ion projected range  $R_p$  was calculated by the SRIM program to be  $34 \pm 12$  nm and  $54 \pm 17$  nm for  $\text{Ar}^+$  implanted at 30 keV and 50 keV, respectively.

*Beyond an expected defect distribution below the ion projected range  $R_d$ , a second defect distribution extending more than two times deeper than  $R_d$  was revealed.*

## Stainless steel exposed to the protons irradiation

SS

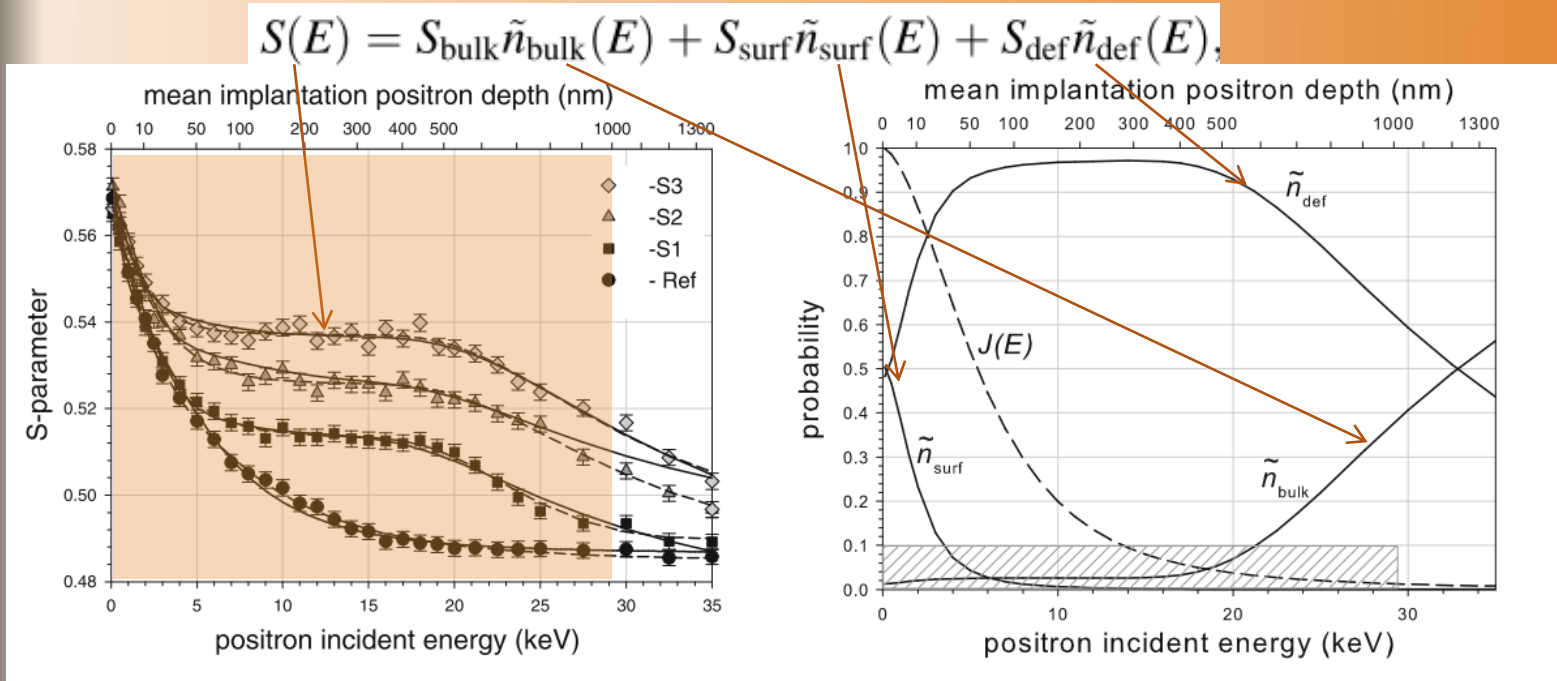
In order to obtain the “rectangular” defect depth profile in stainless steel, i.e., 304 AISI, protons were injected sequentially with different energies from 95 to 220 keV,



# VEP results for SS sample irradiated with protons

SS

Diffusion trapping model for rectangular defect profile.

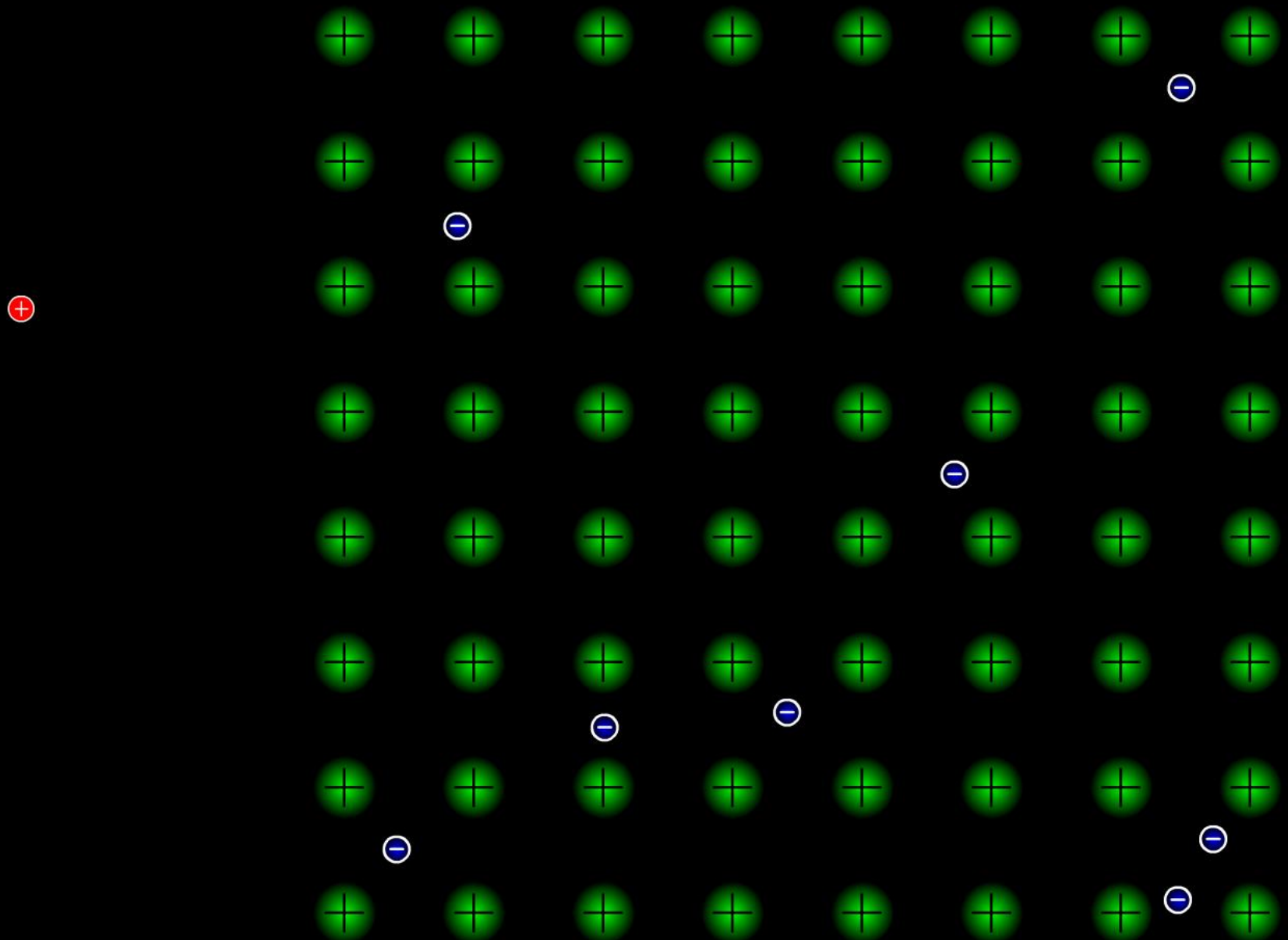


Good agreement between the depths of damaged by energetic protons layers and those obtained from fitting procedure of VEP results was achieved.

## Some remarks regarding the VEP results

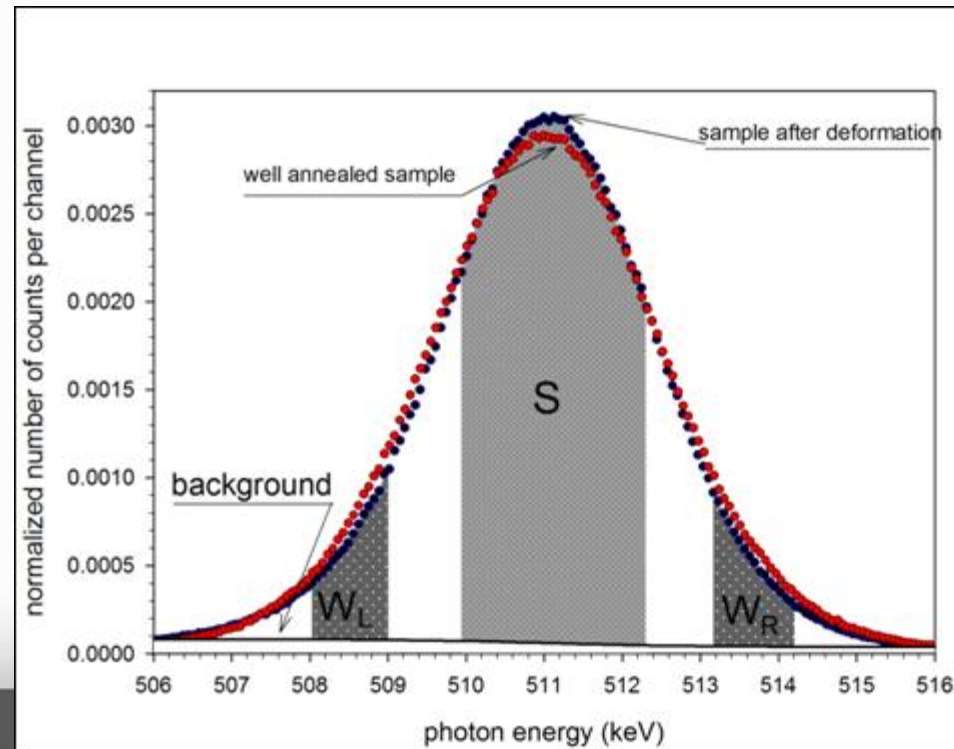
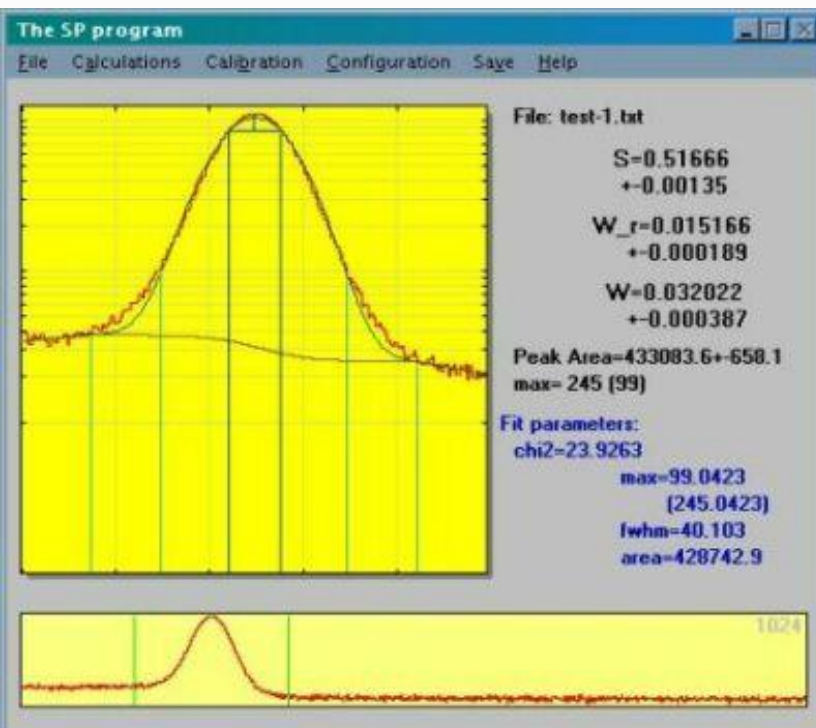
Two reservations about VEP results:

- Positron implantation profile must be known, i.e., Makhovian profile parameters and positron implantation range. These values are determined theoretically, by computer simulations using different codes.
- Defect distribution is convoluted with positron diffusion process. For deconvolution some codes must be used.



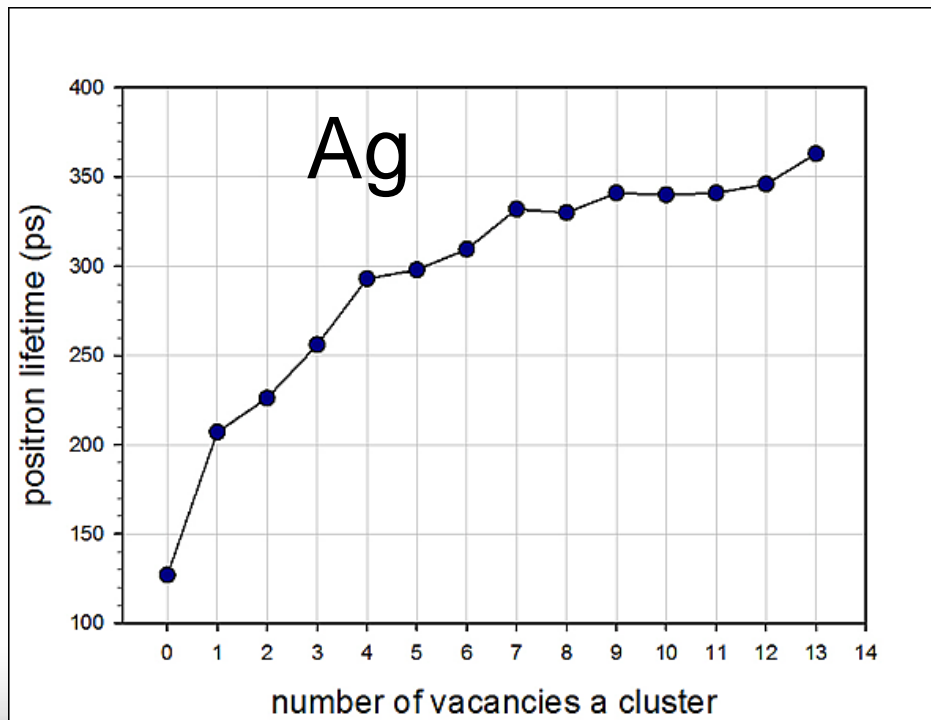
# Spectroscopy of annihilation line

$$E_{\gamma} \cong m_e c^2 - \frac{1}{2} E_b \pm \frac{cp_L}{2} \quad p_F = \hbar \sqrt[3]{3\pi^2 n_e}$$



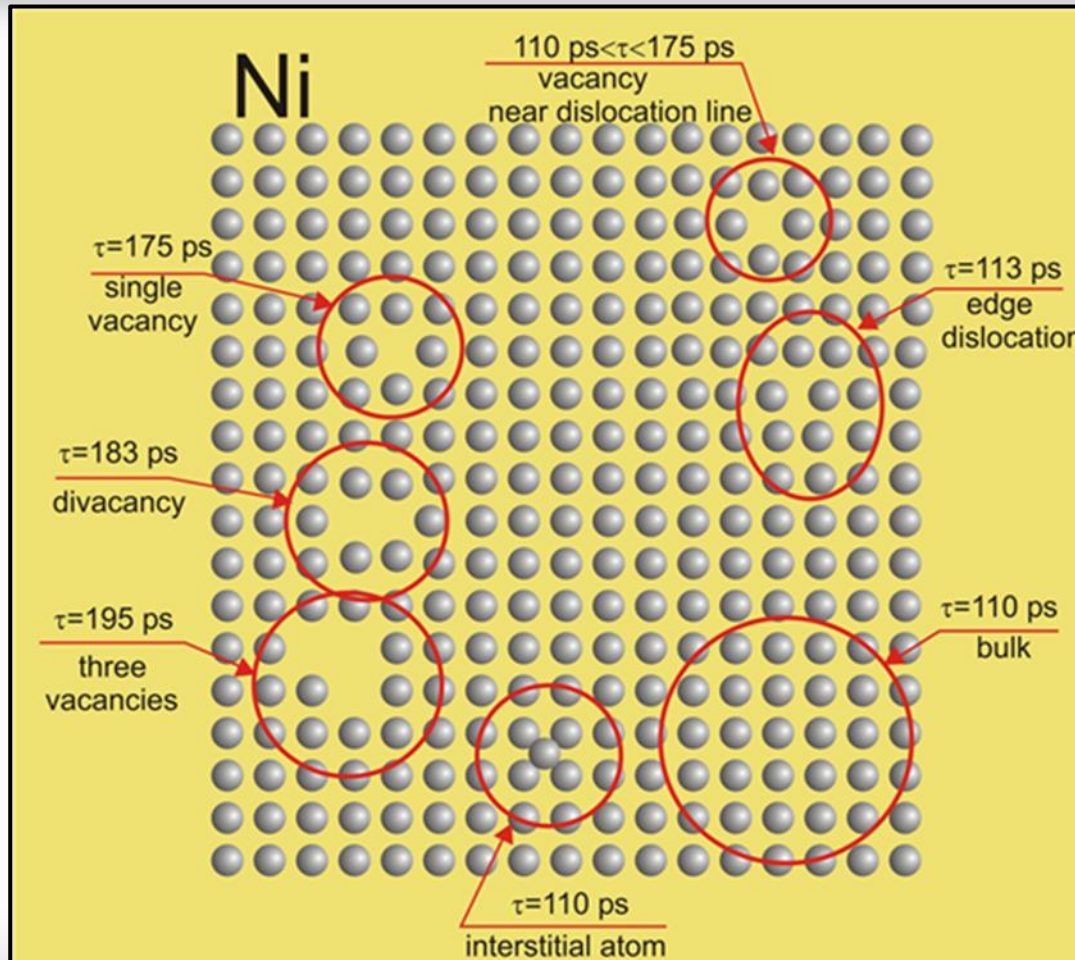
# Positron lifetime spectroscopy

$$\lambda = \frac{1}{\tau} = \pi r_e^2 c \int_{\Omega} d^3 \vec{r} |\Psi_+(\vec{r})|^2 g(\vec{r}, \vec{r}) \left( \sum_j |\psi_j(\vec{r})|^2 \right)$$

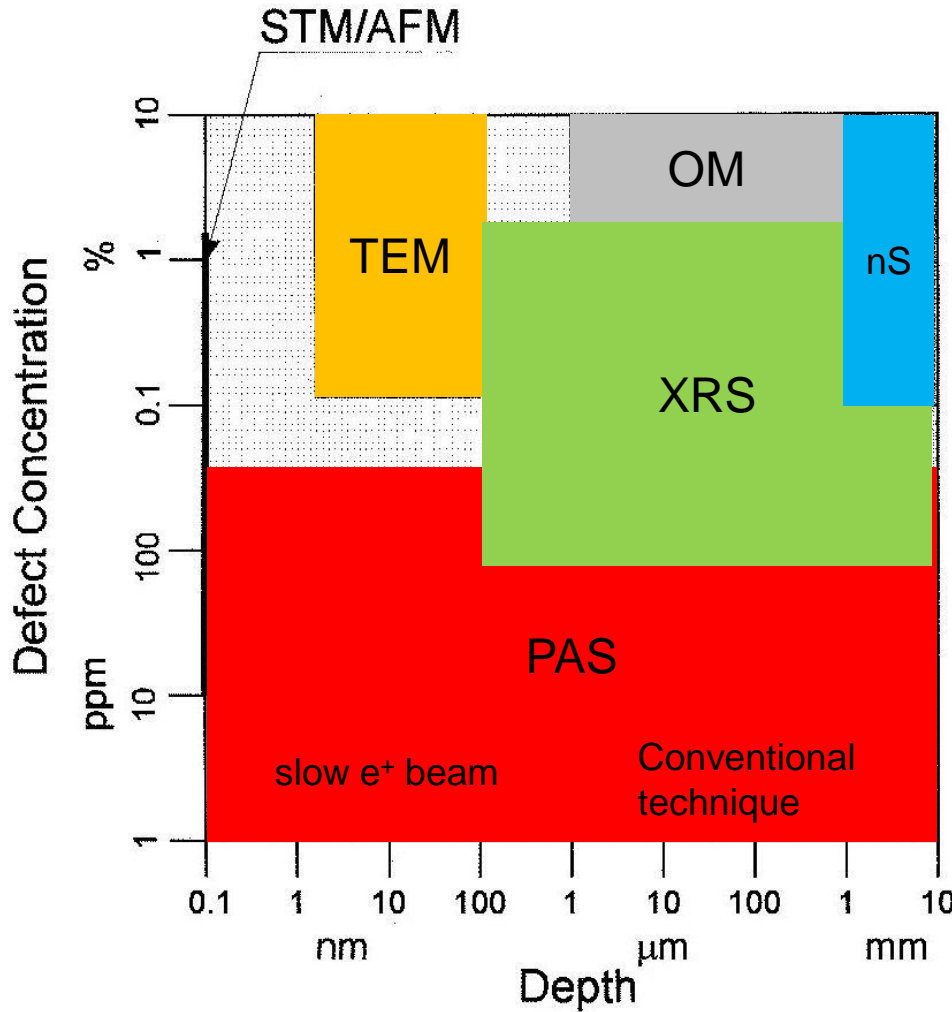


ABINIT code

# Positron lifetime in defects in Ni host



# Sensitivity of positron techniques



**AFM**-atomic force microscopy

**OM**-optical microscopy

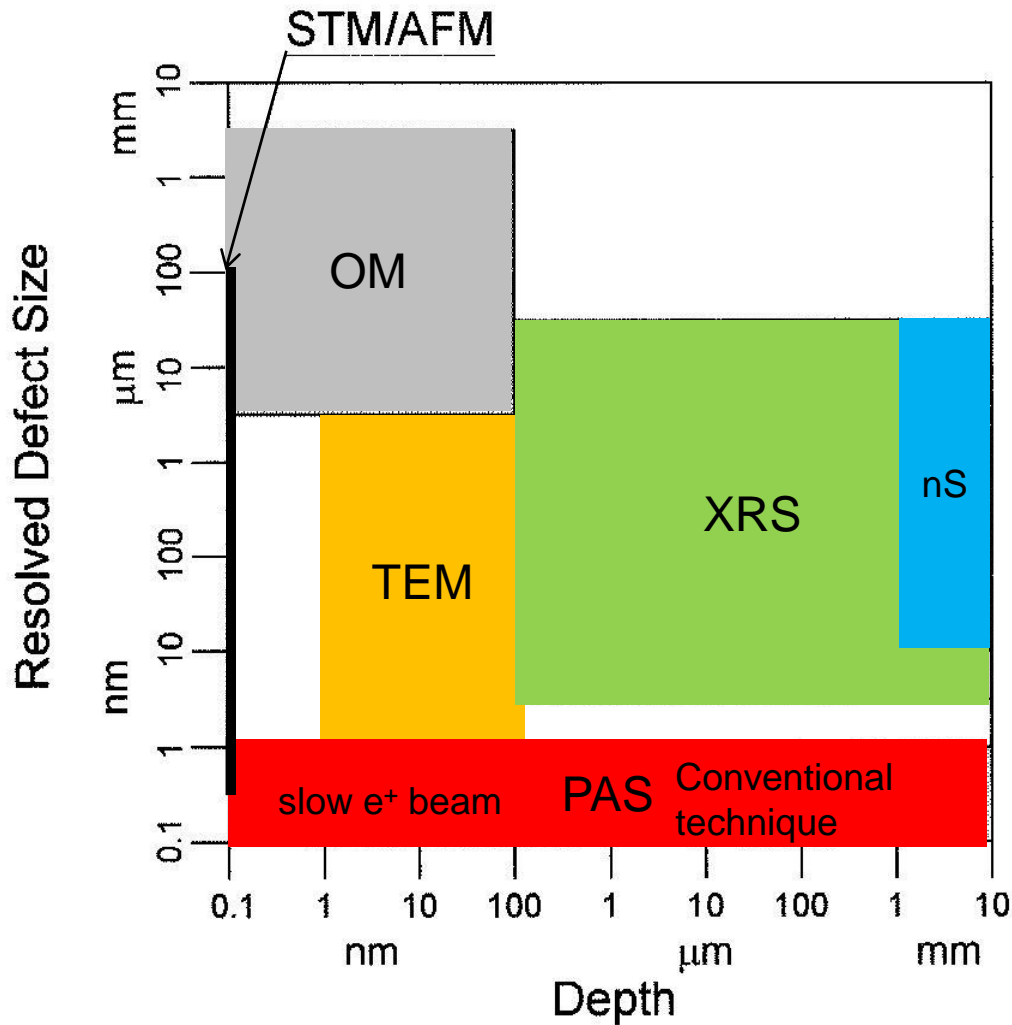
**nS**- neutron spectroscopy

**TEM**-transmission electron microscopy

**XRS**- X-rays spectroscopy

**STM**-scanning tunneling microscopy

# Selectivity of positron techniques



**AFM**-atomic force microscopy

**OM**-optical microscopy

**nS**- neutron spectroscopy

**TEM**-transmission electron microscopy

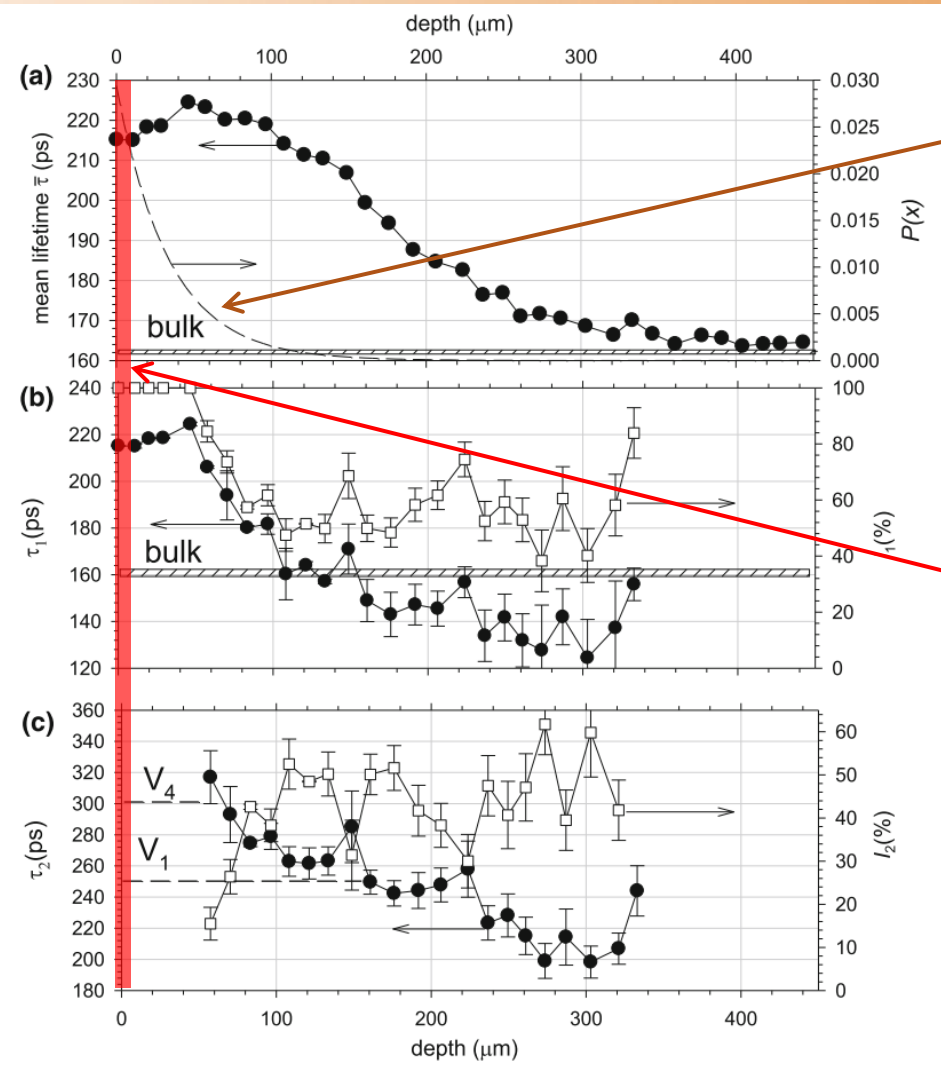
**XRS**- X-rays spectroscopy

**STM**-scanning tuneling microscopy

# Conventional positron measurements for searching of LRE

- Experimental details
- Etching technique
- VEP results
- Results

# Defect profile induced by dry sliding in Zr



Implantation  
profile of  $^{22}\text{Na}$  positrons

Mean positron lifetime

$$\bar{\tau} = I_1 \tau_1 + I_2 \tau_2$$

$$(I_1 + I_2 = 1)$$

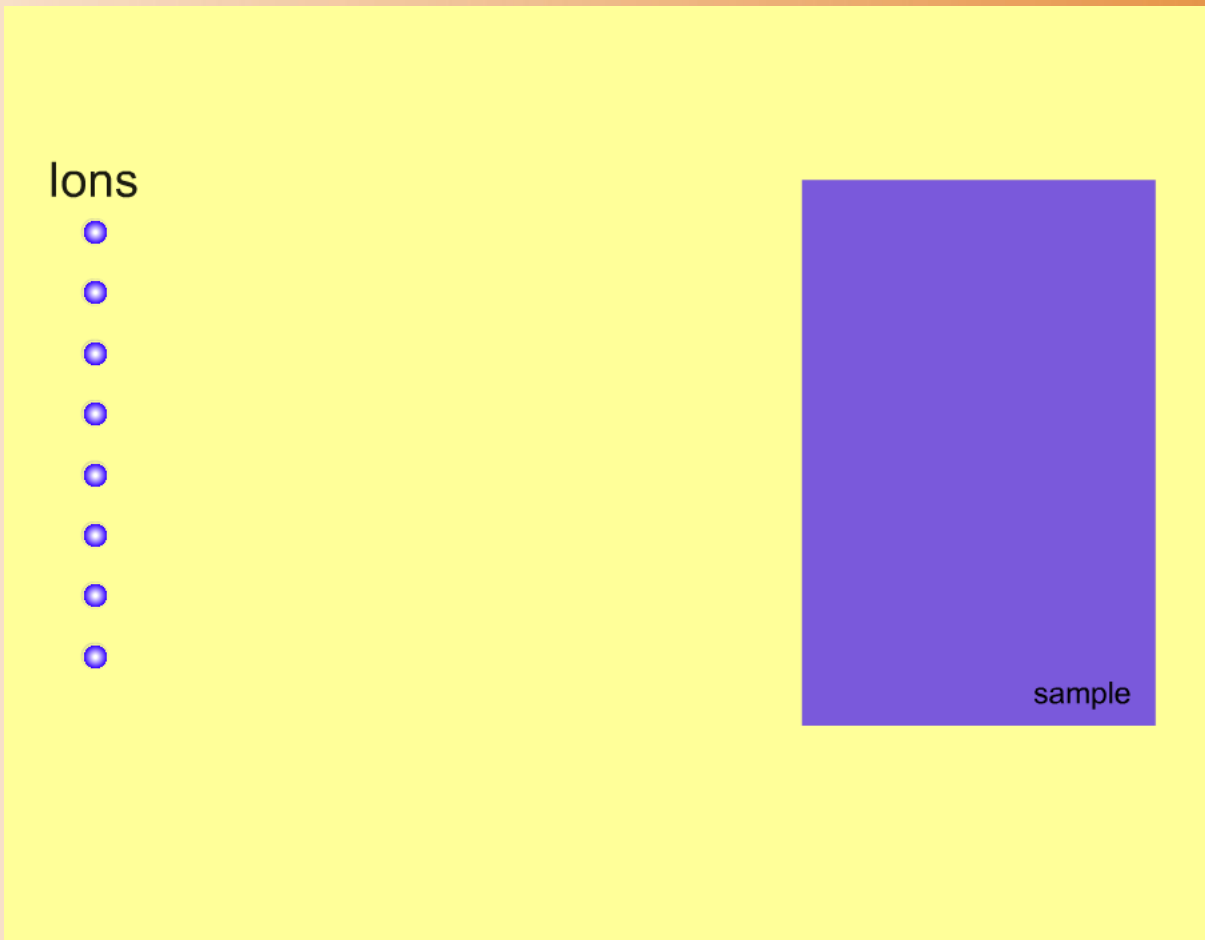
Possible defect profile  
induced by ions  
implantation

## Implantation

- The irradiation was performed at IC-100 cyclotron at Flerov Laboratory of Nuclear Reactions at JINR in Dubna, Russia.  $Xe^{26+}$  heavy ions with energy 167 MeV ions and different dose were applied. The average ion flux was  $5 \times 10^9 \text{ cm}^{-2} \text{ s}^{-1}$ .
- Temperature not higher than 80°C.



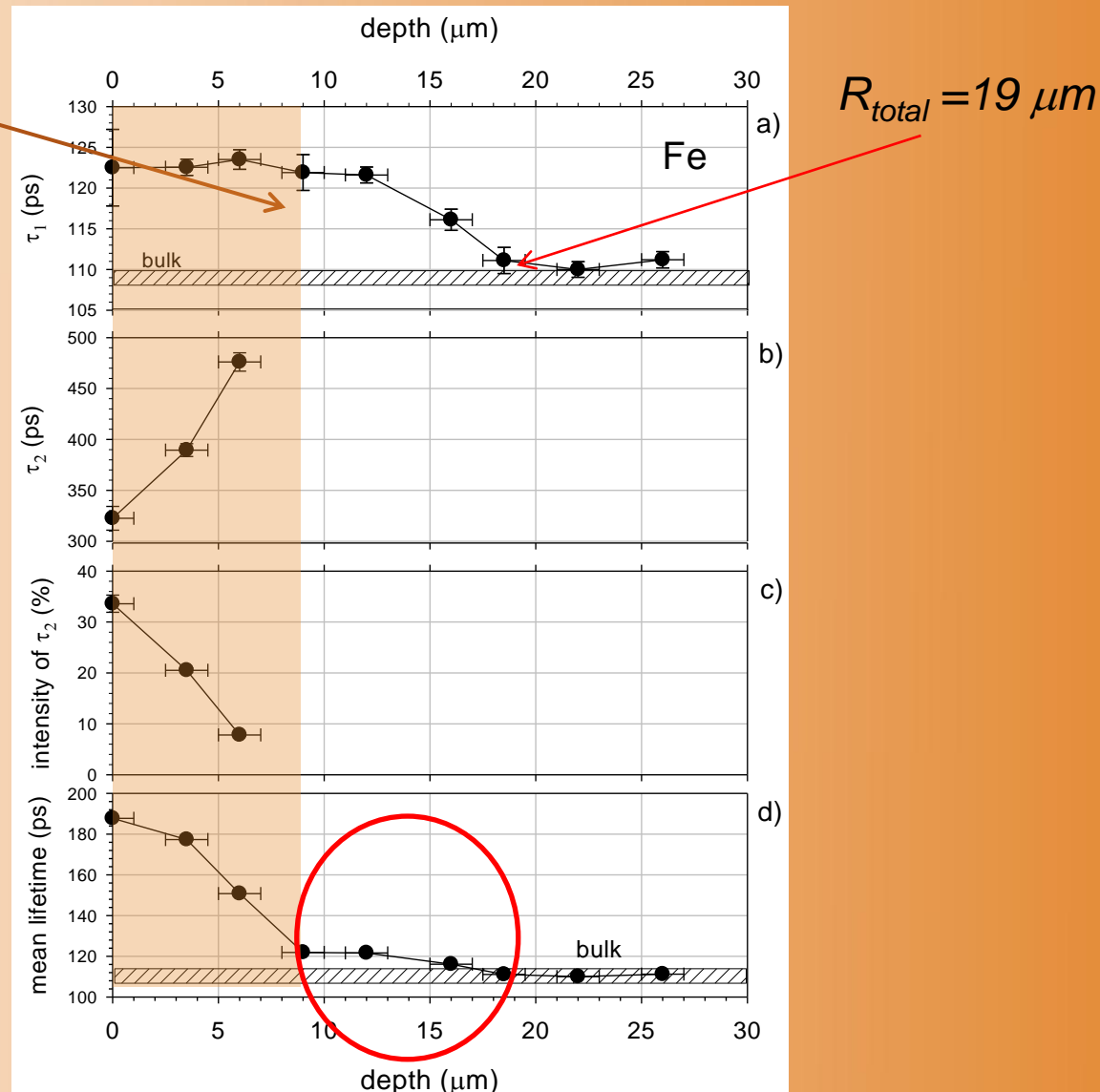
## Experimental technique



Fe

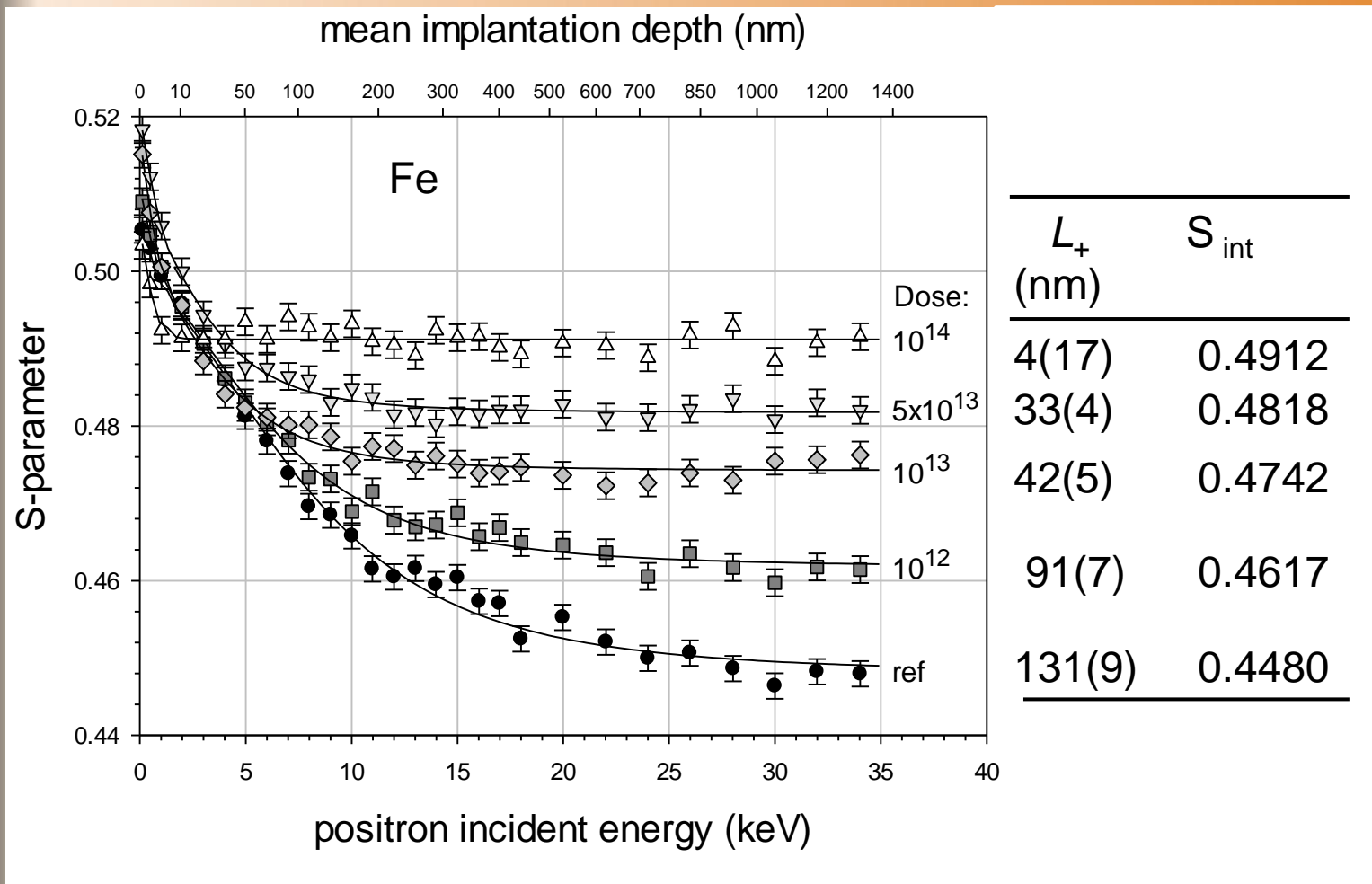
Fe exposed to implantation of 167 MeV Xe<sup>26+</sup>  
dose: 10<sup>14</sup> ions/cm<sup>2</sup>

$$R_p = 8.2 \mu\text{m}$$



# VEP results of Fe irradiated with 167 MeV $Xe^{26+}$ ions

Fe



# Positron diffusion trapping model for VEP experiment

The homogeneous sample with uniformly distributed defects.

S-parameter as a function of incided positron energy:

$$S(E) = S_{\text{int}} + \left( S_{\text{surf}} - S_{\text{int}} \right) \int_0^{\infty} dx p(x, E) \exp\left(-\frac{x}{L_+}\right)$$

$$S_{\text{int}} = \frac{S_{\text{bulk}} \lambda_{\text{bulk}} + S_{\text{def}} k_0}{\lambda_{\text{bulk}} + k_0}$$

$$L_+ = \sqrt{\frac{D_+}{\lambda_{\text{bulk}} + k_0}}$$

$$k_0 = \mu C_V$$

Implantation profile:

$$p(x, E) = \frac{m x^{m-1}}{x_0^m} \exp\left[-\left(\frac{x}{x_0}\right)^m\right]$$

$$x_0 = \frac{A_{1/2}}{\rho (\ln 2)^{1/m}} E^n$$

For silver they are equal as follows (GEANT4):  
 $A_{1/2}=3.27 \text{mg cm}^{-2}\text{keV}^{-n}$ ,  $n=1.576$ ,  $m=1.636^*$

Correction for ephithermal positrons:

$$S'(E) = S(E)[1 - J_{\text{ephi}}(E)] + S_{\text{ephi}} J_{\text{ephi}}(E)$$

$$J_{\text{ephi}}(E) = \int_0^{\infty} dx p(x, E) \exp\left(-\frac{x}{L_{\text{ephi}}}\right)$$

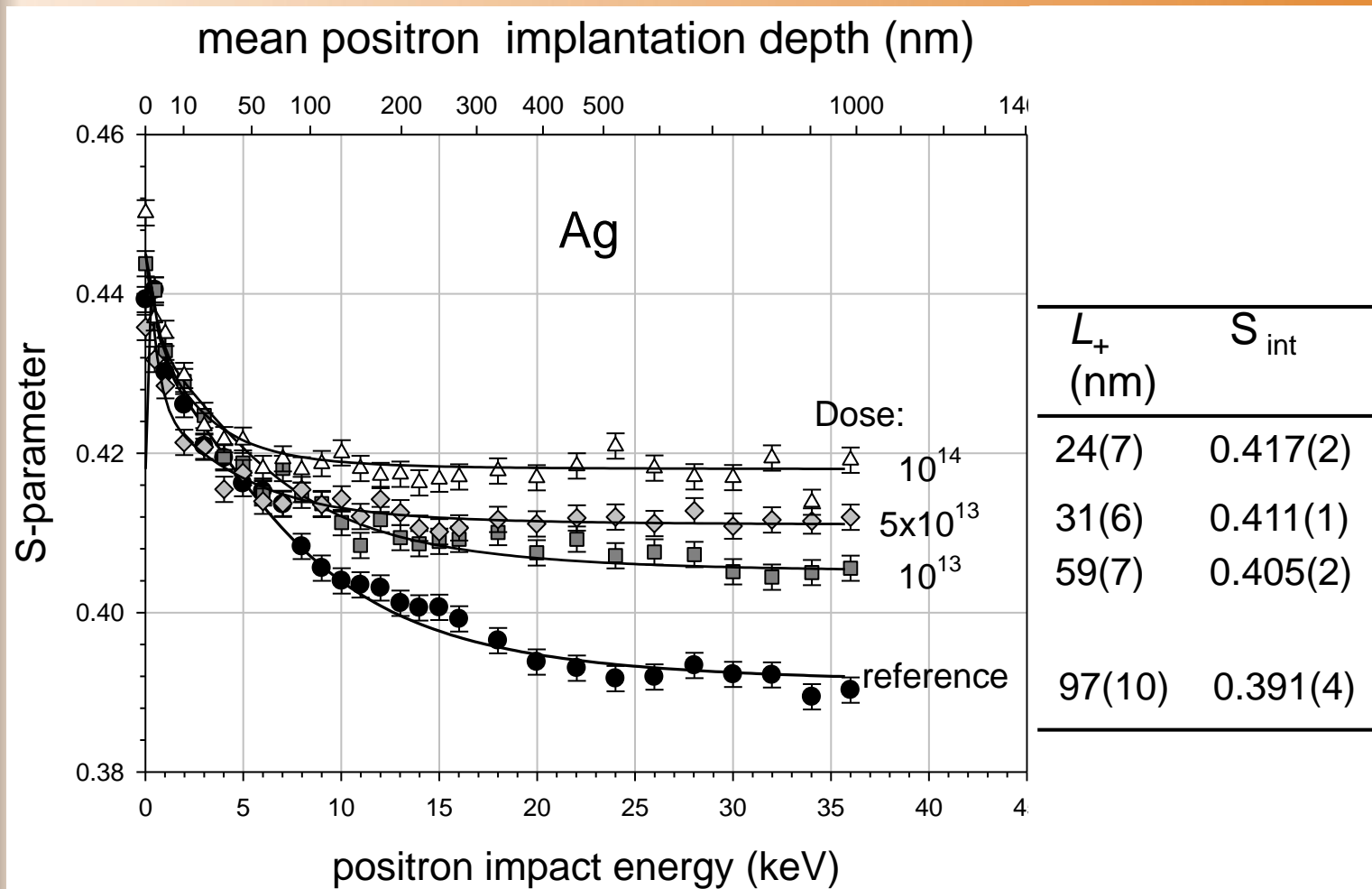
V.A. Stephanovich, J. Dryzek, *Phys. Lett. A* **377** 3038 (2013)

\*J. Dryzek, P. Horodek, *Nucl. Instr. and Meth. in Phys. Res.. B* **266**, 4000 (2008)

J. Dryzek, *Nucl. Instr. and Meth. in Phys. Res.B*, **196**, 186 (2002)

# VEP results of Ag exposed to implantation of 167 MeV Xe<sup>26+</sup>

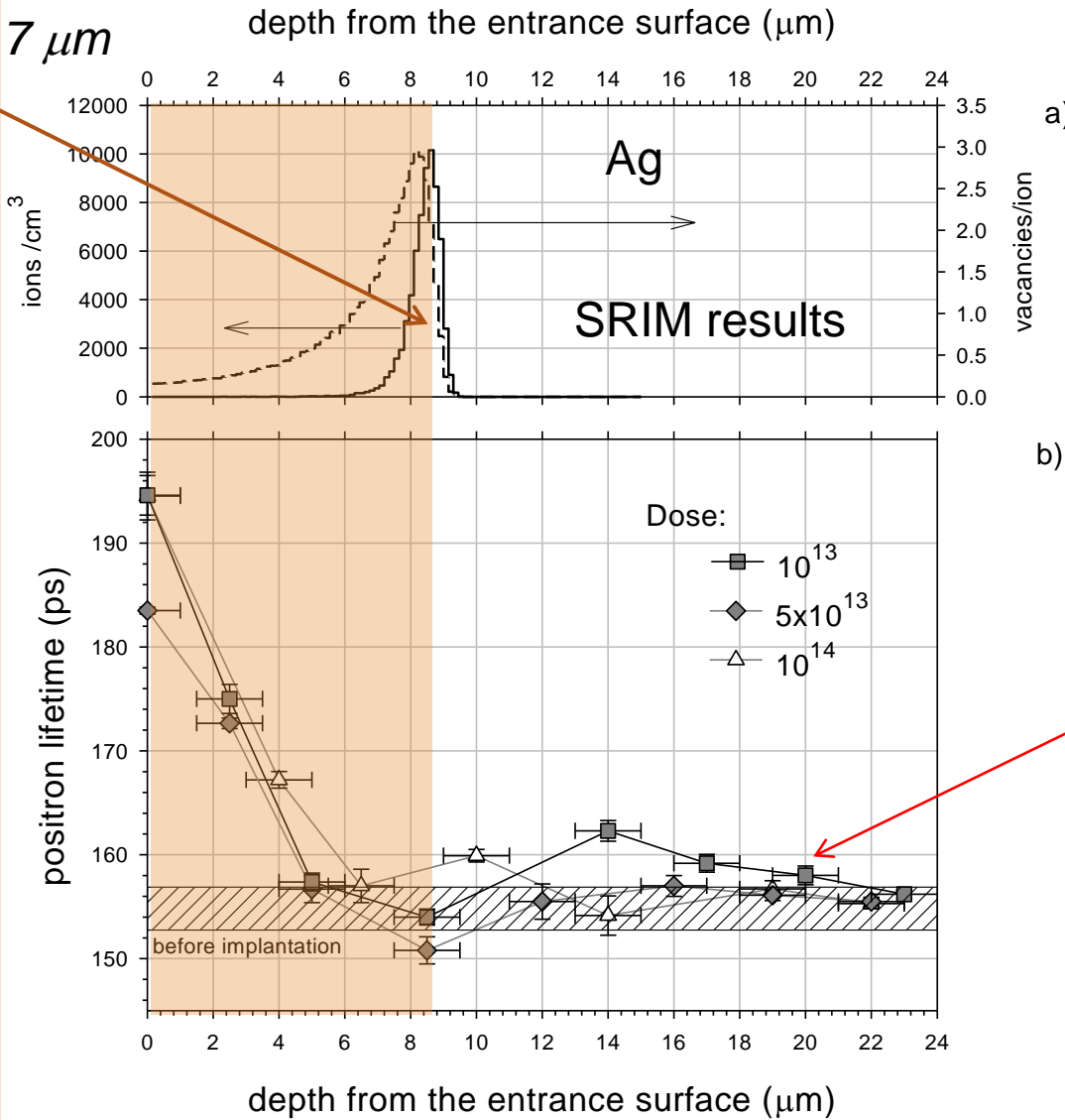
Ag



# Ag exposed to implantation of 167 MeV Xe<sup>26+</sup>

Ag

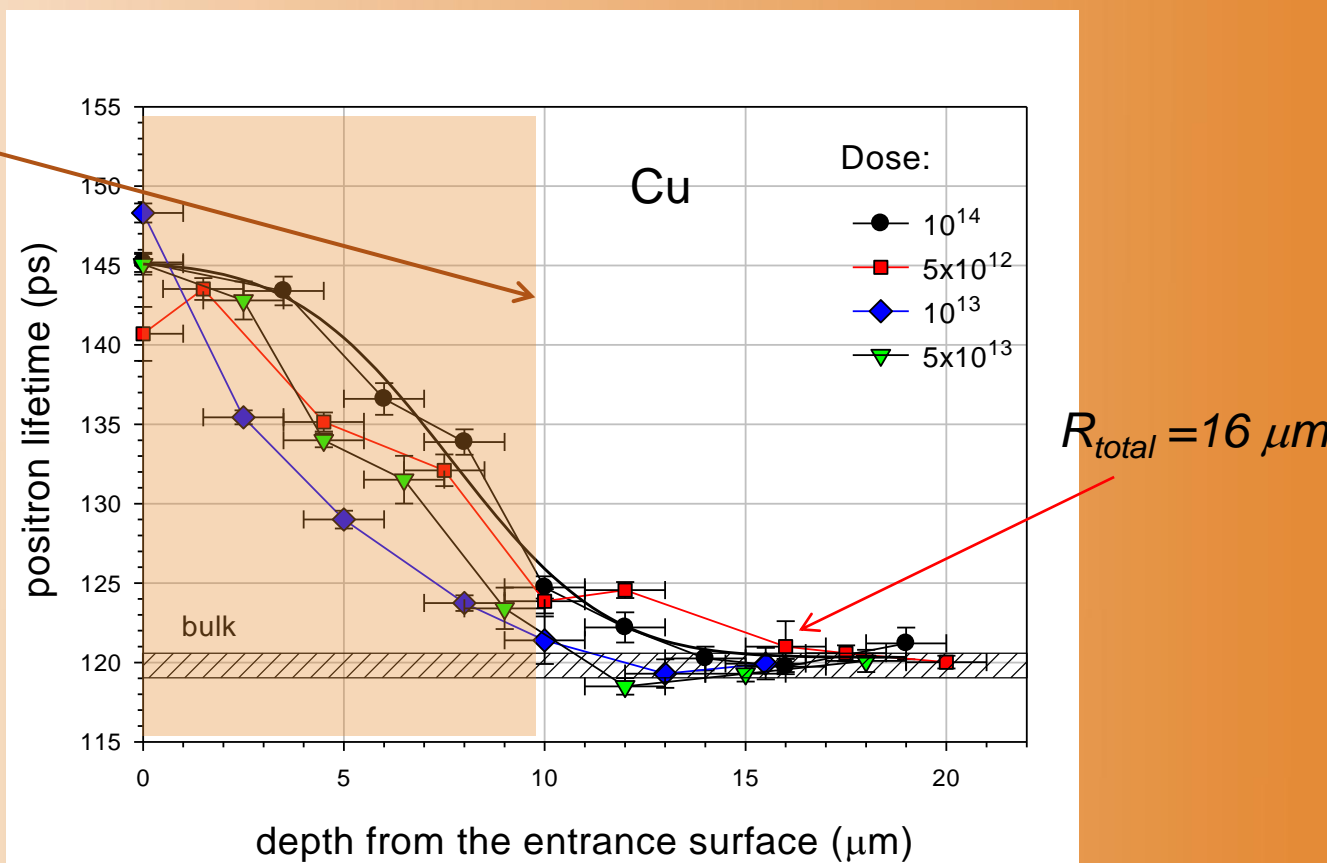
$$R_p = 8.7 \mu\text{m}$$



# Cu exposed to implantation of 167 MeV Xe<sup>26+</sup>

Cu

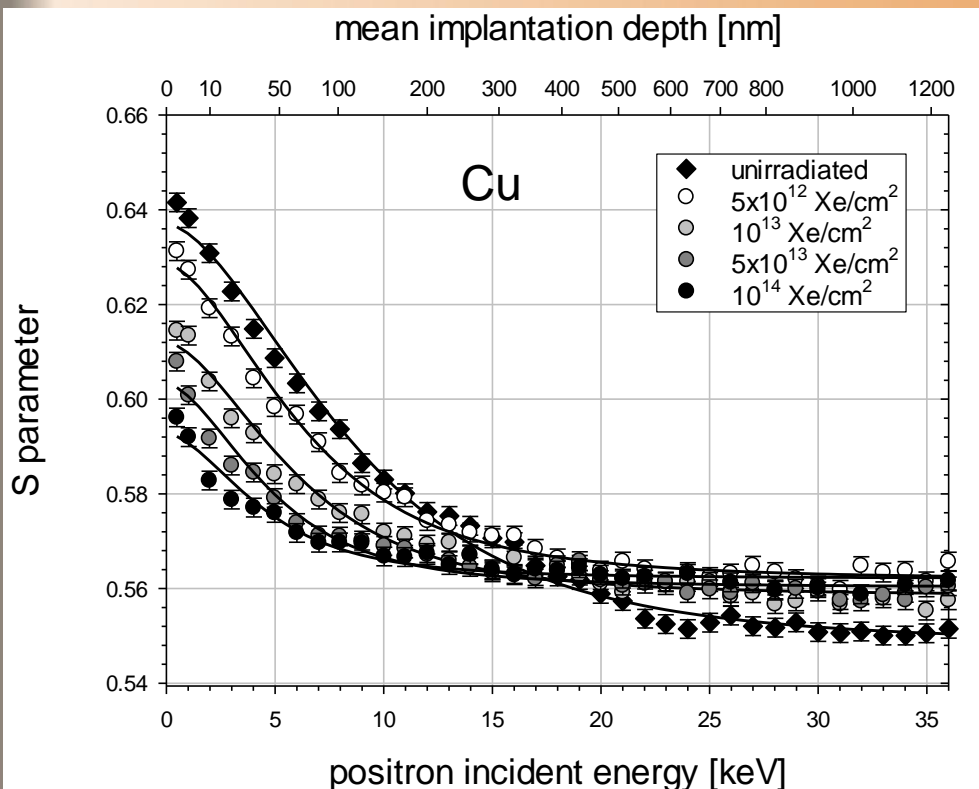
$R_p = 9.5 \mu\text{m}$



$R_{total} = 16 \mu\text{m}$

Cu

## VEP results for Cu irradiated with Xe<sup>26\*</sup> 167 MeV with different dose

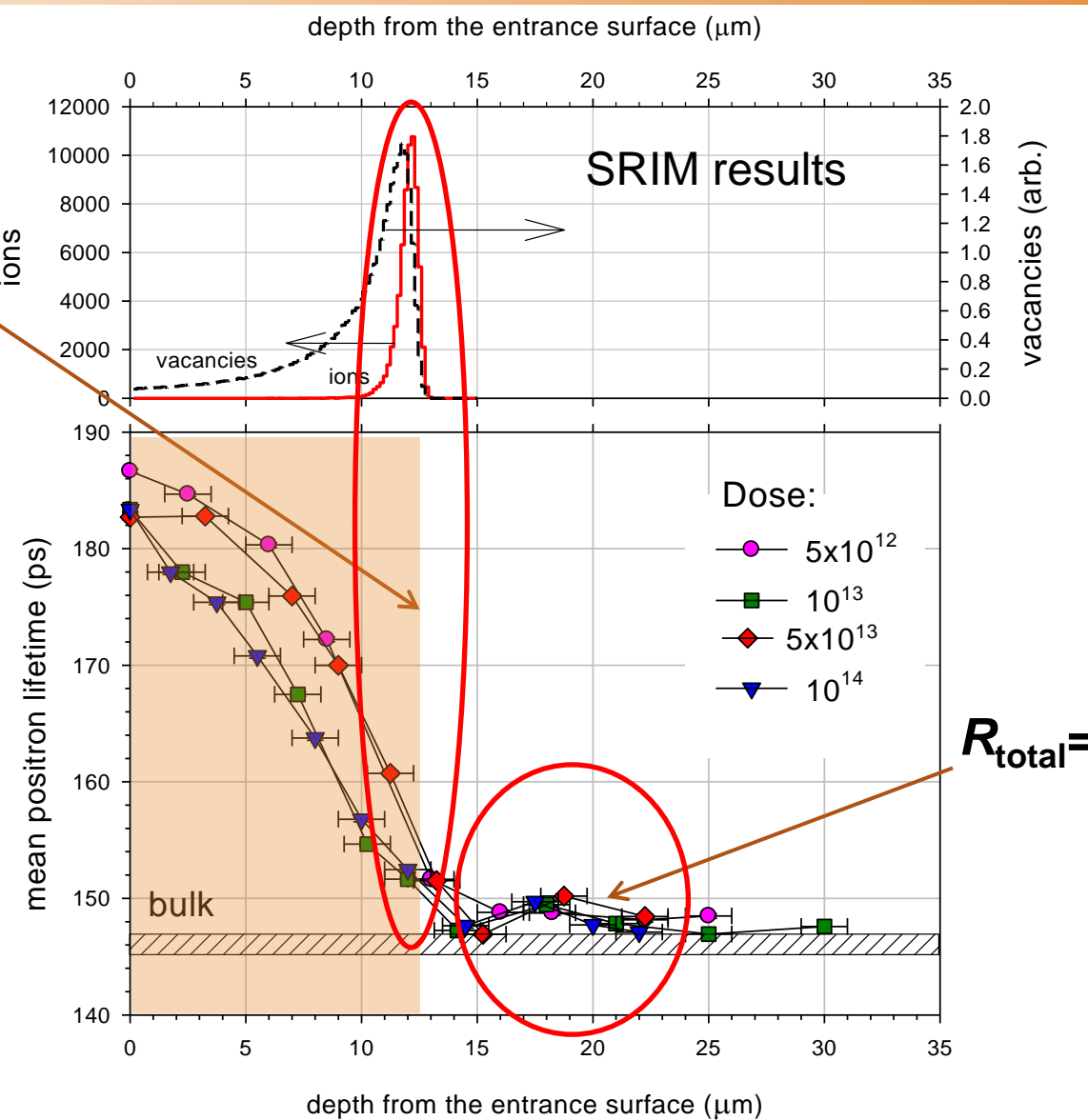


Dose	$L_+$ (nm)	$S_{int}$	$S_{surf}$
Ref.	135(6)	0.548	0.637
$10^{12}$	81(4)	0.562	0.628
$10^{13}$	74(5)	0.558	0.612
$5 \times 10^{13}$	50(5)	0.560	0.603
$10^{14}$	45(6)	0.562	0.592

# Ti irradiated with 167 MeV $\text{Xe}^{26+}$ ions with different dose

Ti

$R_d = 11.8 \mu\text{m}$

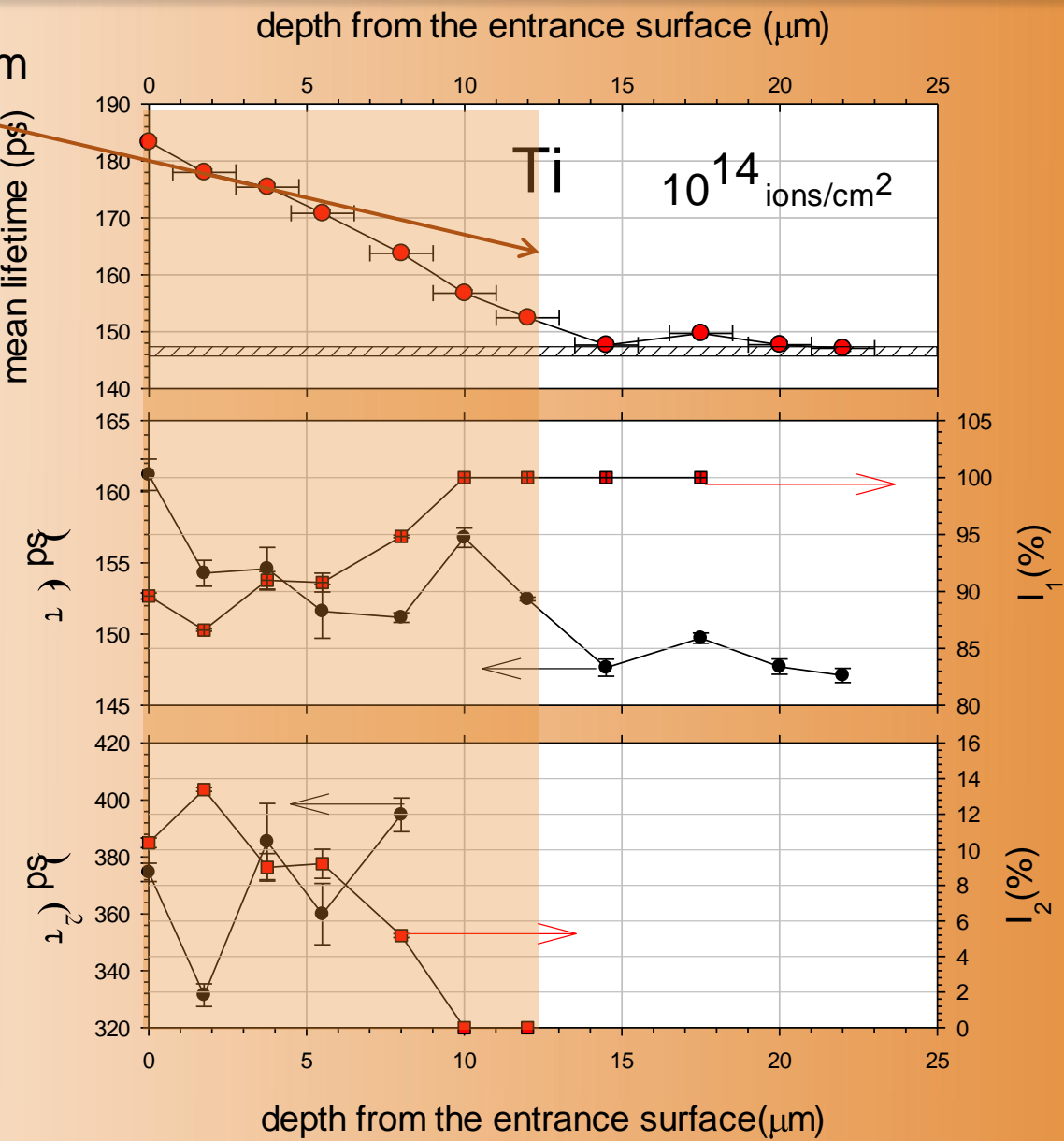


$R_{\text{total}} = 21 \mu\text{m}$

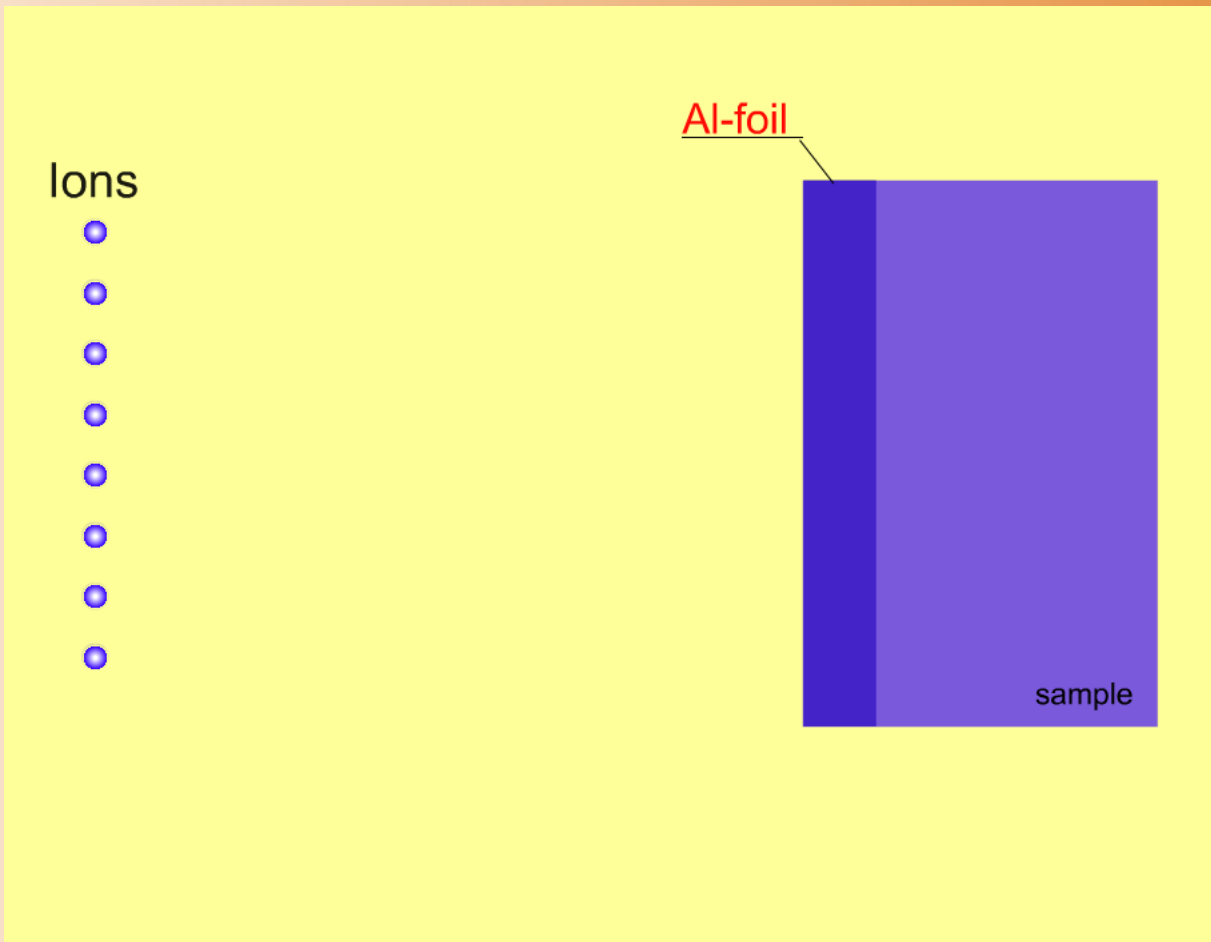
# Ti irradiated with 167 MeV Xe<sup>26+</sup> ions

Ti

$$R_d = 11.8 \mu\text{m}$$



**Thin Al foil allows us to reduce the energy and range of Xe ions in a sample**

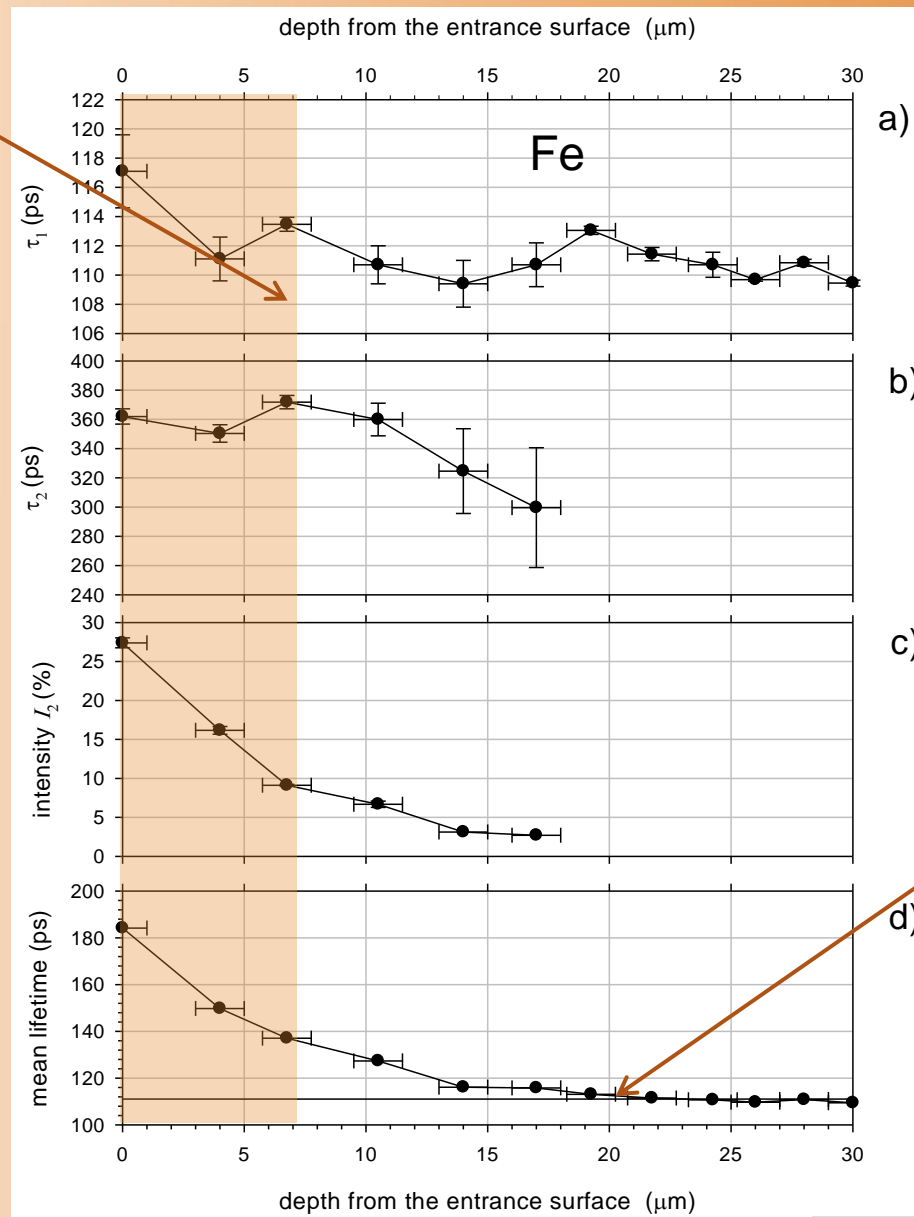


# Fe and Al foil irradiated with 167 MeV Xe<sup>26+</sup> ions

Fe

$R_d=7.1 \mu\text{m}$

Thickness of  
Al foil  $d_{\text{Al}} = 3 \mu\text{m}$



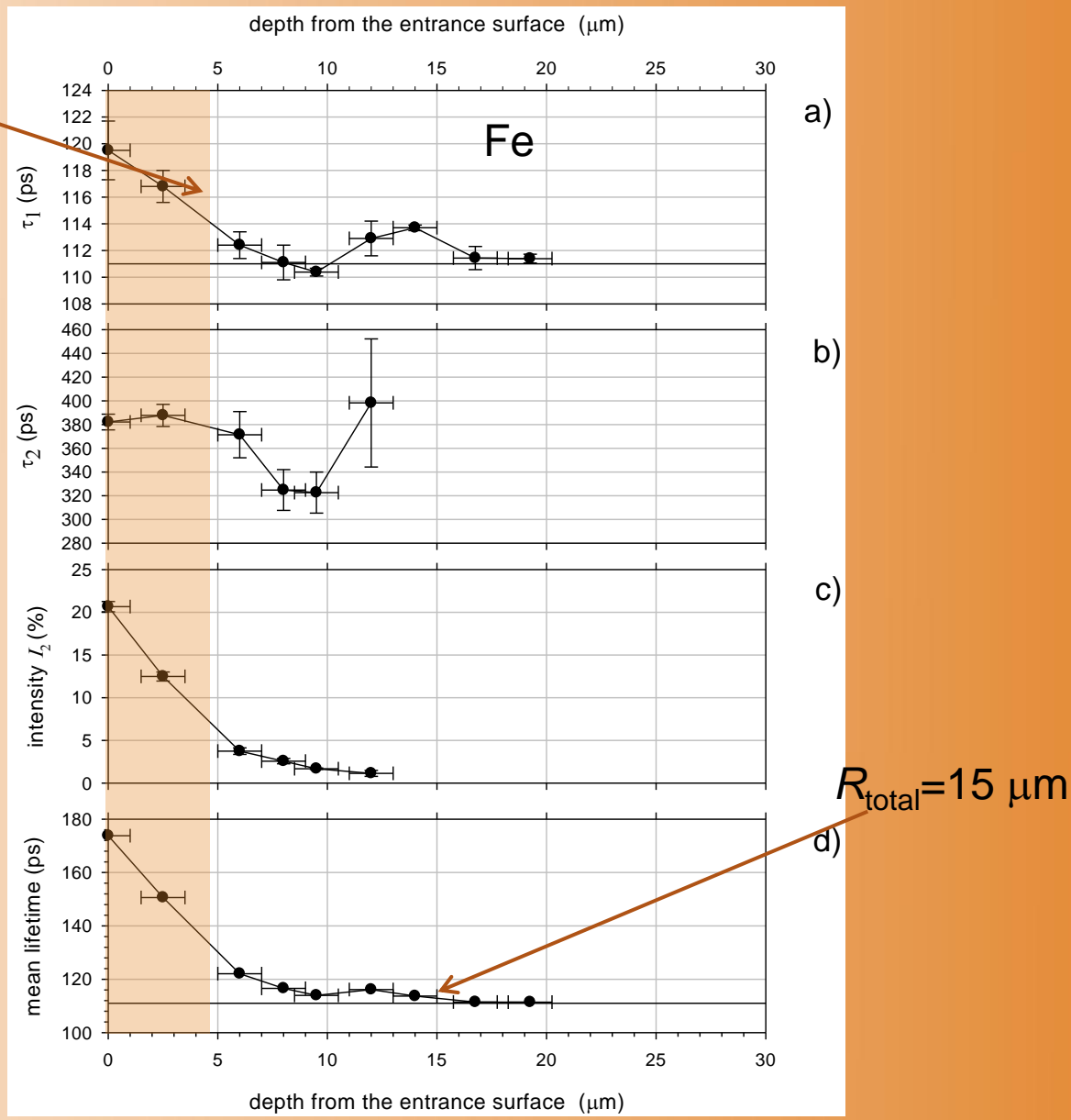
$R_{\text{total}}=19 \mu\text{m}$

# Fe and Al foil irradiated with 167 MeV Xe<sup>26+</sup> ions

Fe

$R_d=4.2 \mu\text{m}$

Thickness of  
Al foil  $d_{\text{Al}} = 9.5 \mu\text{m}$

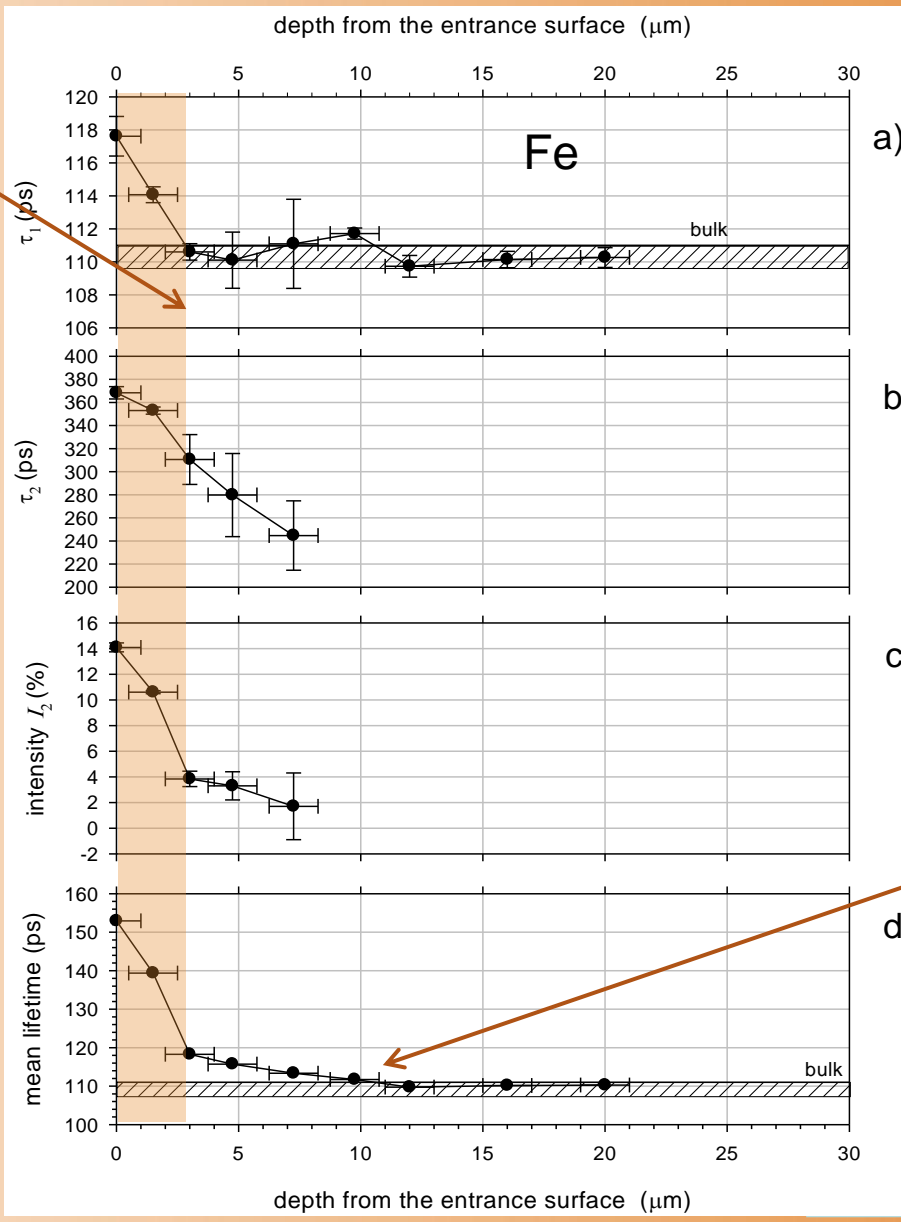


# Fe and Al foil irradiated with 167 MeV Xe<sup>26+</sup> ions

Fe

$R_d = 2.3 \mu\text{m}$

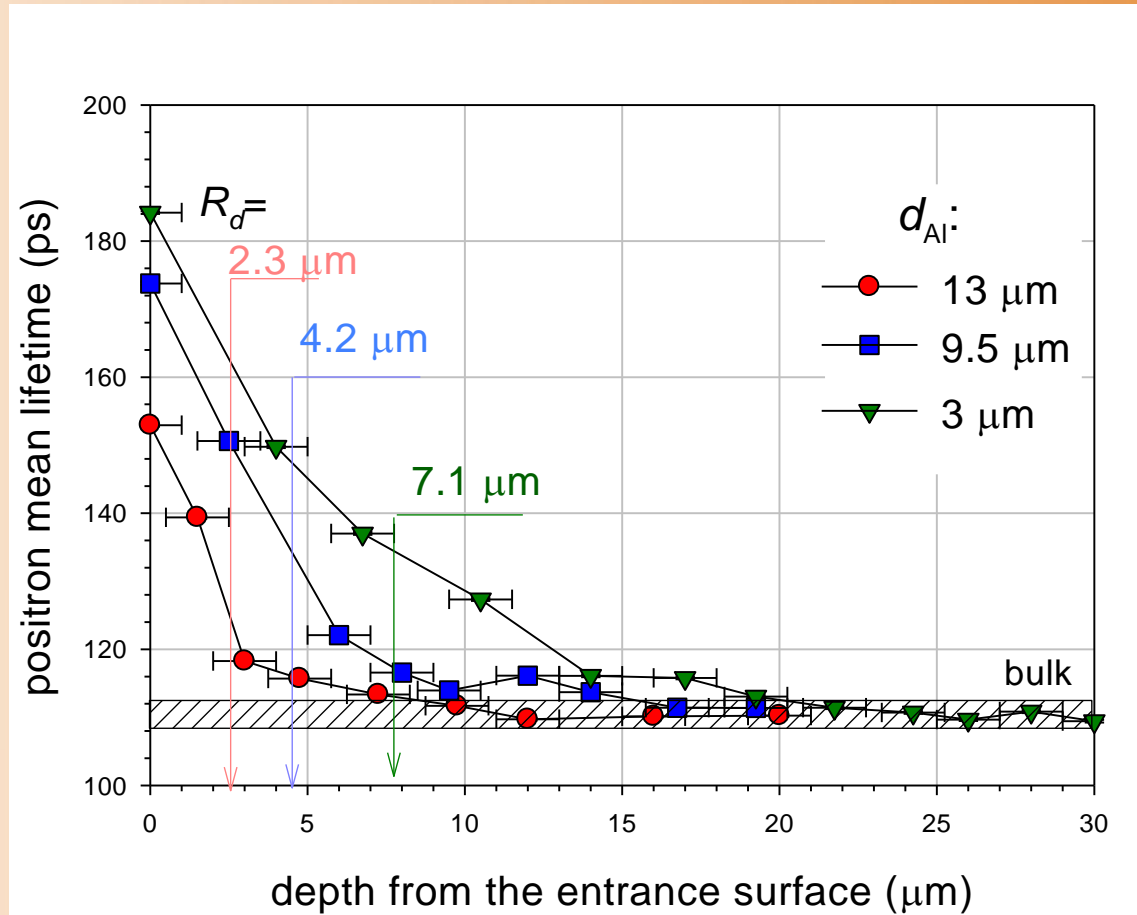
Thickness of  
Al. foil  $d_{\text{Al}} = 13 \mu\text{m}$



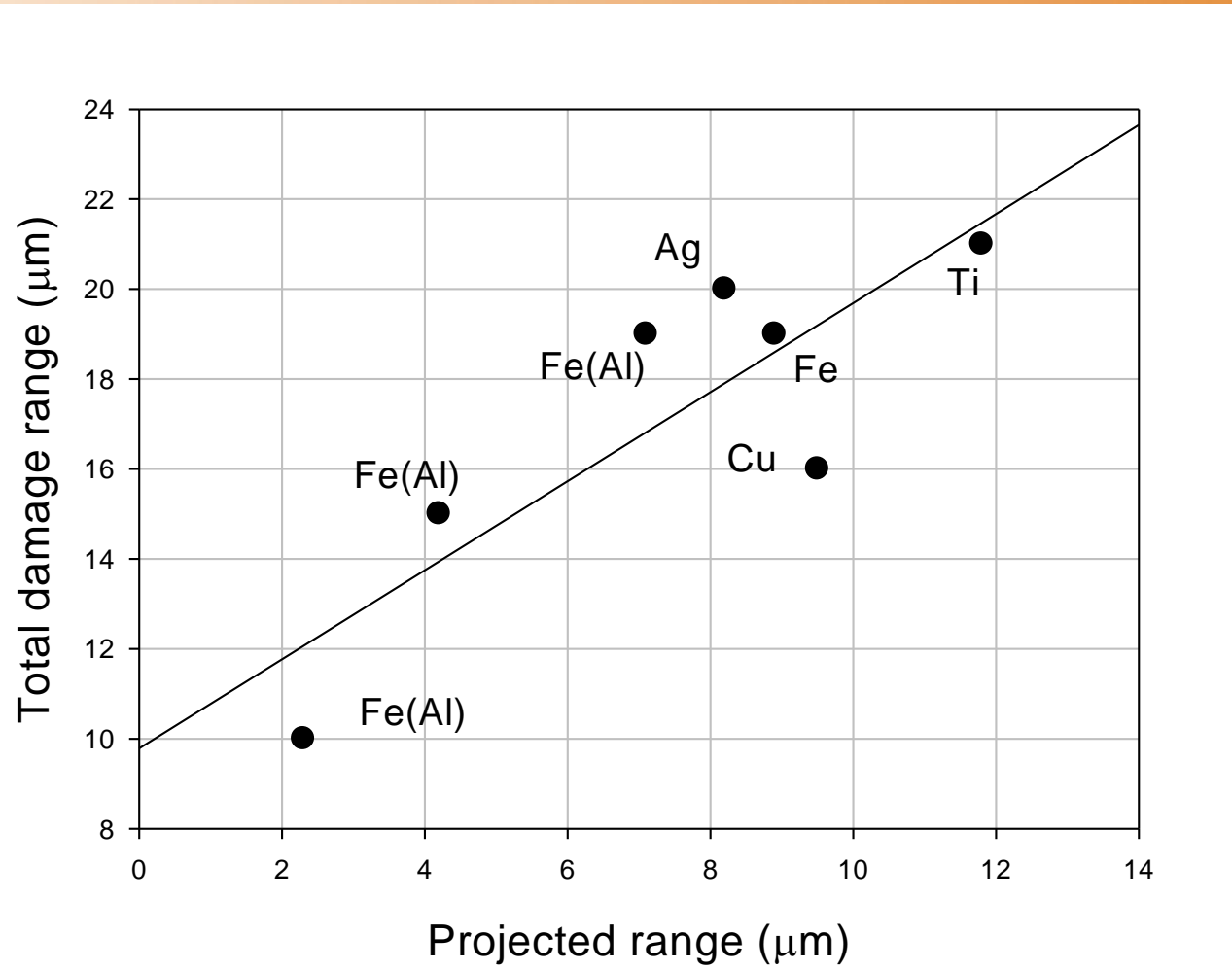
$R_{\text{total}} = 10 \mu\text{m}$

## Fe and Al foil irradiated with 167 MeV $Xe^{26+}$ ions

Fe



## The total damage range vs the projected range

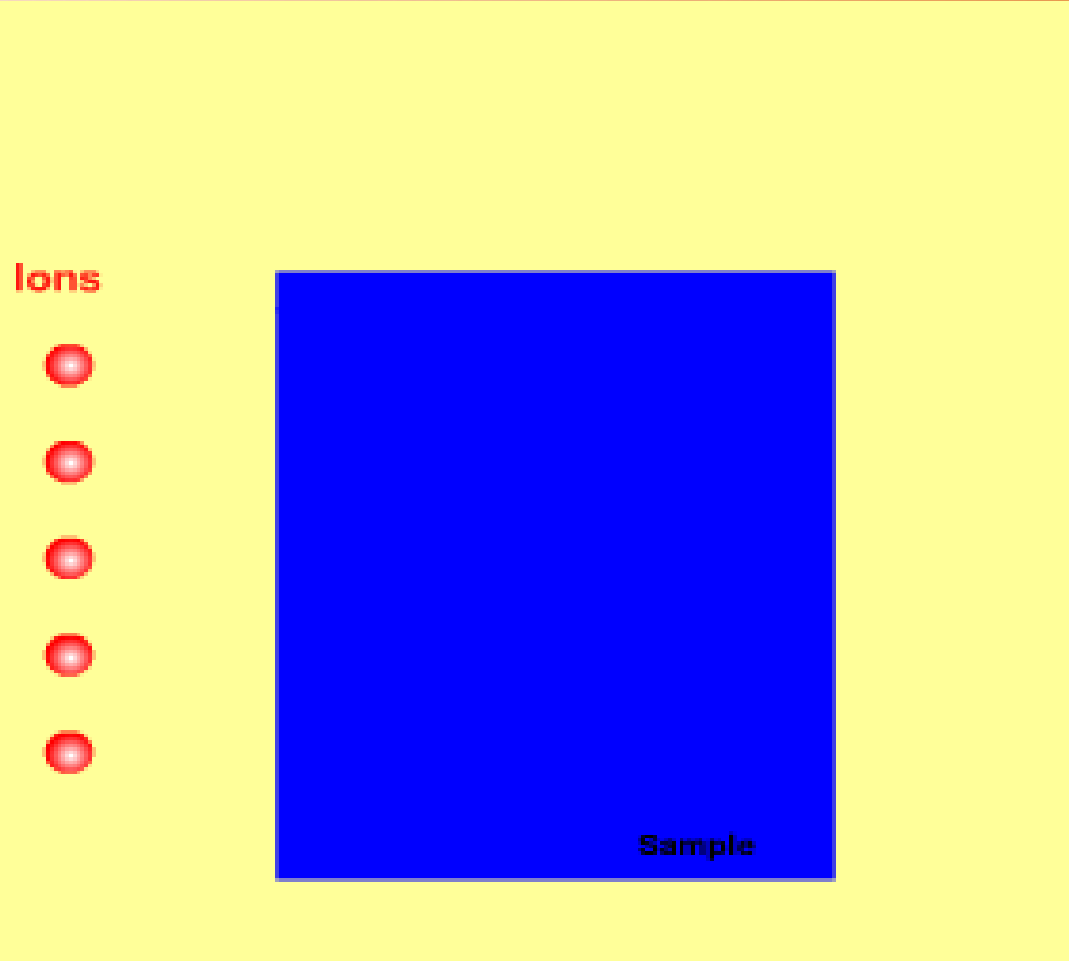


## The damage range beyond the projected range

	Projected range (SRIM) $R_p$ ( $\mu\text{m}$ )	Total damage range (LT) $R_{\text{total}}$ ( $\mu\text{m}$ )	$R_{\text{total}} - R_p$ ( $\mu\text{m}$ )
Ag	8.2	20	<b>11.8</b>
Cu	9.5	16	<b>7.5</b>
Fe	8.9	19	<b>10.1</b>
	7.1	19	<b>11.9</b>
	4.2	15	<b>10.8</b>
	2.3	10	<b>7.7</b>
Ti	11.8	21	<b>9.2</b>

mean: **9.8(5)**  $\mu\text{m}$

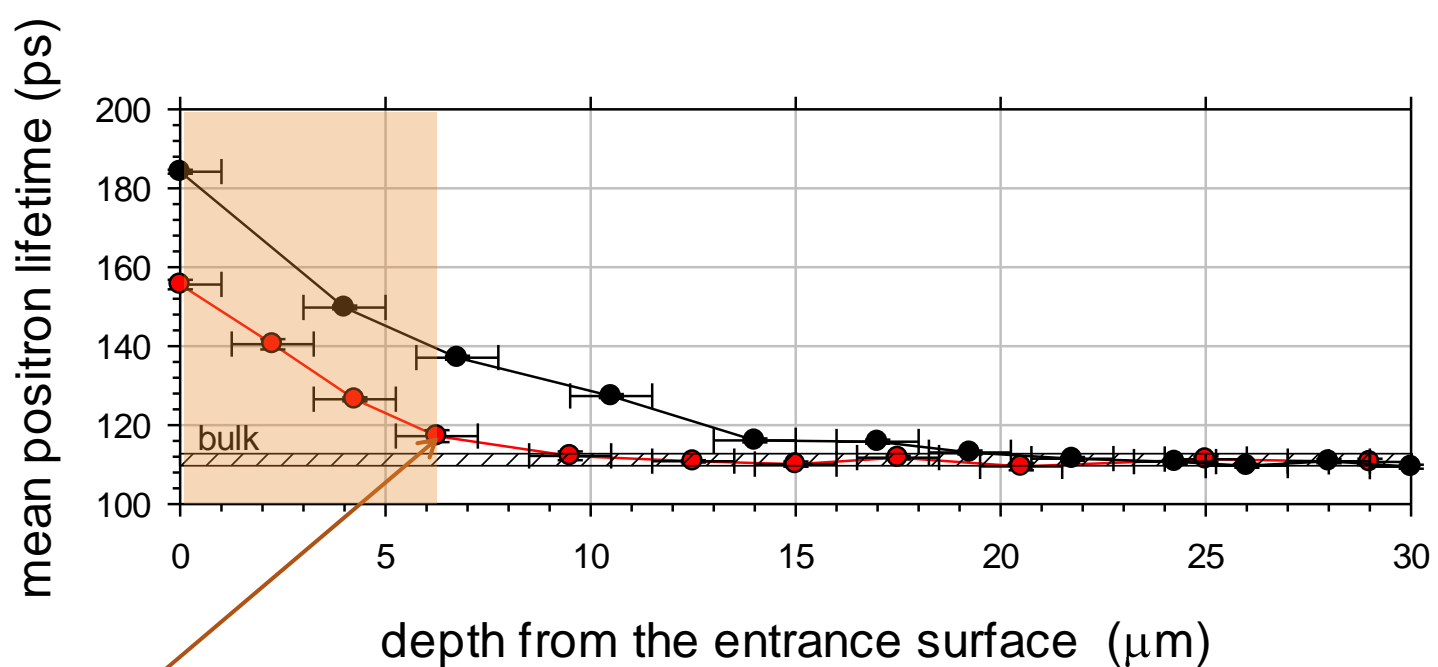
## Origin of the observed effect



Fe

## Fe and Al foil irradiated with 167 MeV $Xe^{26+}$ ions

After annealing at 150 °C during 1 hr, LRE disappears.



Diffusion can be ruled out.

# Conclusions

- For metals: Fe, Cu, Ti, Ag an increase of the mean positron lifetime, indicating presents of defects beyond the  $Xe^{26+}$  ion range is clearly visible.
- The defects beyond the ion range looks like a halo („similar to a halo surrounds the moon”).
- **Long-range effect** observed in our experiments is extended only at the depth of about twice of the projected range.
- No increase of defects concentration at the end of ion range is observed, as it results from SRIM simulations. Adjoined the entrance surface layer is also damaged due to the implantation.
- The proposed etching technique can be applied with succes to studies of defect distribution after swift ion implantation.



Jerzy Dryzek, prof.  
Ewa Dryzek, prof. IFJ  
Paweł Horodek, PhD  
Krzysztof Siemek, PhD  
Konrad Skowron, MSc



A photograph of a mountain range at night under a dark blue sky. The sky is filled with vibrant green and yellow aurora borealis (Northern Lights) that curve elegantly across the frame. The mountains in the foreground are dark and silhouetted against the bright lights of the aurora.

**Thank you for your attention**